Composite Structures 331 (2024) 117910

Contents lists available at ScienceDirect

Composite Structures

journal homepage: www.elsevier.com/locate/compstruct

Bending fatigue behaviour of internal replacement pipe systems

Shanika Kiriella [a], Allan Manalo [a], Cam Minh Tri Tien [a], Hamid Ahmadi [a,*], Patrick G. Dixon [b], Warna Karunasena [a], Ahmad Salah [a], Brad P. Wham [b]

[a] *Centre for Future Materials, University of Southern Queensland, Toowoomba, QLD 4350, Australia*
[b] *Center for Infrastructure, Energy, and Space Testing, University of Colorado Boulder, CO 80309, United States*

A R T I C L E I N F O

Keywords:
Internal replacement pipe (IRP)
Gas pipelines
Repetitive traffic loading
Finite element analysis
Stress-life method
Multiple regression analysis

A B S T R A C T

Internal replacement pipe (IRP) systems are becoming an effective rehabilitation technique for legacy oil and gas pipelines with defects and discontinuities. Under repetitive traffic loads, the IRP-repaired pipes are subjected to fatigue. However, existing knowledge on the fatigue behaviour and remaining service life of IRP systems with circumferential discontinuities under cyclic bending is limited. Therefore, this paper investigated numerically the bending fatigue behaviour of legacy pipelines with circumferential discontinuities rehabilitated with IRP made from various material systems. The influence of the discontinuity width of the host pipe, thickness and elastic modulus of IRP, and level of traffic loading on the fatigue behaviour is evaluated. The results show that the tensile stress concentration at the discontinuity edge controls the bending fatigue behaviour of fully bonded IRP. The critical stresses and the minimum fatigue lifetimes are considerably influenced by the thickness and elastic modulus of the IRP systems, and the level of traffic loading while the width of the circumferential discontinuity has an insignificant effect. Multiple regression analyses show that the level of the traffic load has the most significant effect on the critical stress generated in the IRP, while the largest contribution to the minimum fatigue life comes from the elastic modulus of the repair material.

1. Introduction

Hydrocarbons, including crude oil, natural gas, and liquid petroleum products, are the primary sources of global energy and are directly related to economic growth [1]. Despite being the most common method of transporting oil and gas for over a century, pipelines, predominately composed of cast iron and steel, have the potential to fail during their service life for various reasons [2,3]. According to several studies [4–9], corrosion has been identified as the primary cause of pipeline failure, which can result in circumferential cracks and discontinuities in the host pipes [10]. Corrosion can result in a reduction in wall thickness, strength, and structural integrity of the pipes and can lead to accidents caused by leakage [6,11]. Circumferential cracks in buried pipelines can also be produced by external loadings such as earth load, traffic load, and soil movement [12]. The failure of gas and oil pipelines can lead to substantial financial losses for the energy industry and can cause irreversible damage to both human life and the environment [13]. Consequently, the rehabilitation of damaged pipelines is crucial to prevent them from exacerbating into more significant problems.

The traditional pipeline repair techniques mainly involve replacing the pipes via excavation [14,15]. However, due to financial concerns, it is usually preferable to repair damaged pipes using trenchless rehabilitation techniques rather than replacing them [16]. The internal replacement pipe (IRP) system is an advanced and efficient trenchless rehabilitation technology that has recently been integrated into the pipeline industry [17,18]. This repair method entails the installation of a new structural pipe inside existing legacy pipes which contain defects and discontinuities. During the installation process, the outer surface of IRP is bonded to the inside of the cleaned and prepared host pipe [19]. The implementation of IRP contributes to improving the strength, structural integrity and durability of the existing legacy pipes. However, the application of this technology in rehabilitating legacy gas pipelines has been limited due to the absence of established design procedures and design standards. Hence, it is essential to undertake an in-depth investigation of the structural performance of new and emerging IRP systems under different loading conditions.

* Corresponding author.
E-mail addresses: shanika.kiriella@unisq.edu.au (S. Kiriella), allan.manalo@unisq.edu.au (A. Manalo), camminhtri.tien@unisq.edu.au (C.M.T. Tien), hamid.ahmadi@unisq.edu.au (H. Ahmadi), padi9036@colorado.edu (P.G. Dixon), karu.karunasena@unisq.edu.au (W. Karunasena), ahmad.salah@unisq.edu.au (A. Salah), brad.wham@colorado.edu (B.P. Wham).

https://doi.org/10.1016/j.compstruct.2024.117910
Received 21 August 2023; Received in revised form 14 December 2023; Accepted 11 January 2024
Available online 17 January 2024

Dixon et al [20] have identified nine potential performance objectives that should be taken into consideration for the effective design of IRP systems for rehabilitating legacy gas pipelines. These objectives include cyclic in-service surface loads, lateral deformation, hoop stress, axial deformation, cross-sectional ovalization, puncture, debonding, service connections and compatibility with current and future gas compositions. According to the study conducted by Tafsirojjaman et al [17], cyclic in-service surface loads have been identified as a significant factor that impacts the performance of IRP systems. Repetitive surface loads often arise from overhead vehicular traffic [21] and might induce dynamic fatigue stresses, potentially resulting in the failure of the repair system [17,19,20,22–24]. Additionally, offshore pipelines are vulnerable to fluctuating loads initiated by waves and currents, resulting in catastrophic damage [25–30]. Fatigue can cause a material to accumulate damage, leading to cracking or complete failure at a stress lower than its ultimate strength [31,32]. A detailed understanding of fatigue behaviour and accurate life estimation of IRP systems, therefore, is an important aspect of IRP design and development.

Despite the significance of implementing safe design practices to prevent bending fatigue failure of IRP caused by repetitive surface loading, there is a lack of extensive research in this area. The existing experimental studies on the bending fatigue behaviour of circumferential discontinuities or joint repairs are restricted to a few repair systems, specifically those utilizing low-modulus CIPP liners or SAPL [19,22,23]. Jeon et al [22] studied the behaviour of a cured-in-place pipe (CIPP) lining system in cast iron (CI) host pipe with a complete circumferential crack subjected to repetitive heavy traffic loading over 50 years of design life. The test results showed that the internal vertical stiffness of the pipe lining decreased by approximately 75 % after 1 million cycles of deformation. Throughout the testing, the liner was able to endure relative displacement and rotation caused by heavy traffic loads at circumferential cracks without breaking. However, localized debonding between the interfaces of the CI host pipe and liner near the circumferential crack was observed. According to Jeon et al [22], this localised debonding right near the crack edge benefits the liner by improving flexibility and decreasing the stress concentration. Under a similar approach, Stewart et al [19] examined the performance of CI pipes with a joint repaired by a CIPP liner subjected to one million cycles of deflections, which was equivalent to traffic loading over 50 years of the service life. During the testing, the liner experienced the greatest relative deformation and rotation at the discontinuity of the CI pipe. However, the rotational stiffness of the system remained almost constant over one million cycles. Additionally, the level of deflection applied in these two studies [19,22] was estimated from an analytical model developed by Jeon et al [22] and O'Rourke et al [33], respectively under the assumption that the stiffness of the liner is negligible. Recent studies [17,20] have indicated that this simplification can lead to the under-utilisation of relatively stiffer new and emerging IRP materials. Ha et al [23] performed a three-point cyclic bending test on a steel host pipe with a circumferential crack repaired using a polyurea-polyurethane spray-applied pipe lining (SAPL). During testing, the liner demonstrated a stiffness reduction but no indication of leakage or failure. However, the motivation behind the investigation conducted by Ha et al [23] was not explicitly stated as the traffic load. It can be noted that these previous works rely on expensive and time-consuming full-scale experiments and cover very limited parameters that can influence the fatigue behaviour of pipe liners in bending.

IRP repair systems are currently being developed employing a variety of materials such as polymers (both thermosets and thermoplastics), composites, and metallic materials [17,18]. Many investigations have demonstrated that the fatigue performance of these materials varies substantially due to the differences in their strength, stiffness, toughness and resistance to cracking and fracture [34–39]. As compared to composites and metals, most polymeric materials have lower tensile strength, modulus of elasticity (MOE), and toughness, which can have a major impact on their fatigue resistance [40–44]. FRP composites, on the other hand, can exhibit outstanding fatigue performance because of their high strength, and stiffness. [36,45]. In contrast to metal fatigue, the loss of stiffness in composite materials can be observed from the early stage of the fatigue loading process [46,47]. Further, compared to polymers, metallic materials have higher MOE and toughness, which contributes to their excellent fatigue performance [48]. However, metallic materials, are prone to corrosion, which may diminish their fatigue resistance over time [49]. Therefore, a detailed evaluation of the structural performance of IRP systems made from different materials is required to ensure that they will be in operation throughout their design life.

There are some attempts in doing numerical simulations of internal repair systems in the literature. Tafsirojjaman et al [17] conducted finite element analyses (FEA) to investigate the fatigue behaviour of an IRP alone subjected to repetitive vehicular traffic loads by utilising the stress-life approach. This study evaluated IRP materials with MOE ranging from 1 GPa (145 ksi) to 200 GPa (29,008 ksi) and repair thicknesses varying from 3.175 mm (0.125 in) to 25.4 mm (1 in), assuming a design life of one million cycles. The findings of this study showed that an increase in thickness and MOE of IRP can lead to a significant extension of the fatigue life. The influence of repair thickness, repair material, and discontinuity width on the static bending behaviour of IRP-repaired discontinuous legacy steel pipes exposed to surface load from vehicular traffic was studied by Kiriella et al [50]. The results of this initial study showed that when the discontinuity is narrow, the host pipe has the most effect on the lateral deformation behaviour of the system, while IRP has a larger influence when the discontinuity is wider. Additionally, the impact of the repair thickness and repair material on the lateral deformation behaviour is dependent upon the width of the host pipe discontinuity. Therefore, the findings of this study highlight the importance of conducting a numerical investigation to understand how different parameters affect the bending fatigue behaviour in the presence of host pipes with circumferential discontinuities.

Shou and Chen [51] and Yang et al [52] conducted numerical studies on CIPP-rehabilitated pipe subjected to bending caused by vehicular traffic loading, which was validated through full-scale experimental testing [53]. These studies developed three-dimensional FE models that incorporated surrounding soil. However, they did not account for the cyclic nature of the traffic loading and solely considered surface corrosion defects on the host pipe rather than full circumferential discontinuities. According to Yang et al [52], the thickness of the CIPP liner was identified as the most critical parameter affecting the stress development in the liner. In their respective studies, Brown et al [54] and Tien et al [18] investigated numerically the effect of the discontinuity edge of CI host pipe on the performance of a CIPP liner and a thermoplastic IRP, respectively, under internal pressure. These studies revealed that the application of internal pressure results in the concentration of axial stress in the repair pipe at the edge of the host pipe discontinuity. Tien et al [18] has further explained that this phenomenon occurs due to IRP curving around the host pipe discontinuity. However, the effect of discontinuity edge on stress concentration may vary depending on the loading condition. Therefore, it is necessary to investigate these effects under the cyclic bending condition.

The literature review reveals a scarcity of extensive numerical studies on the bending fatigue performance of IRP systems in the presence of legacy pipes with full circumferential discontinuities. Also, there is a lack of understanding of the potential effect of various design parameters on the bending fatigue behaviour of IRP systems, which is crucial for ensuring long-term structural integrity and reliability. Therefore, the present study investigated numerically the fatigue behaviour of IRP systems used for repairing host pipes with circumferential discontinuities at the midspan under repeated traffic loading. The investigation considered both the mechanical contribution of the IRP and the potential impact resulting from the presence of discontinuous legacy pipe segments. Additionally, the study also evaluated the influence of different parameters identified from previous studies, such as the

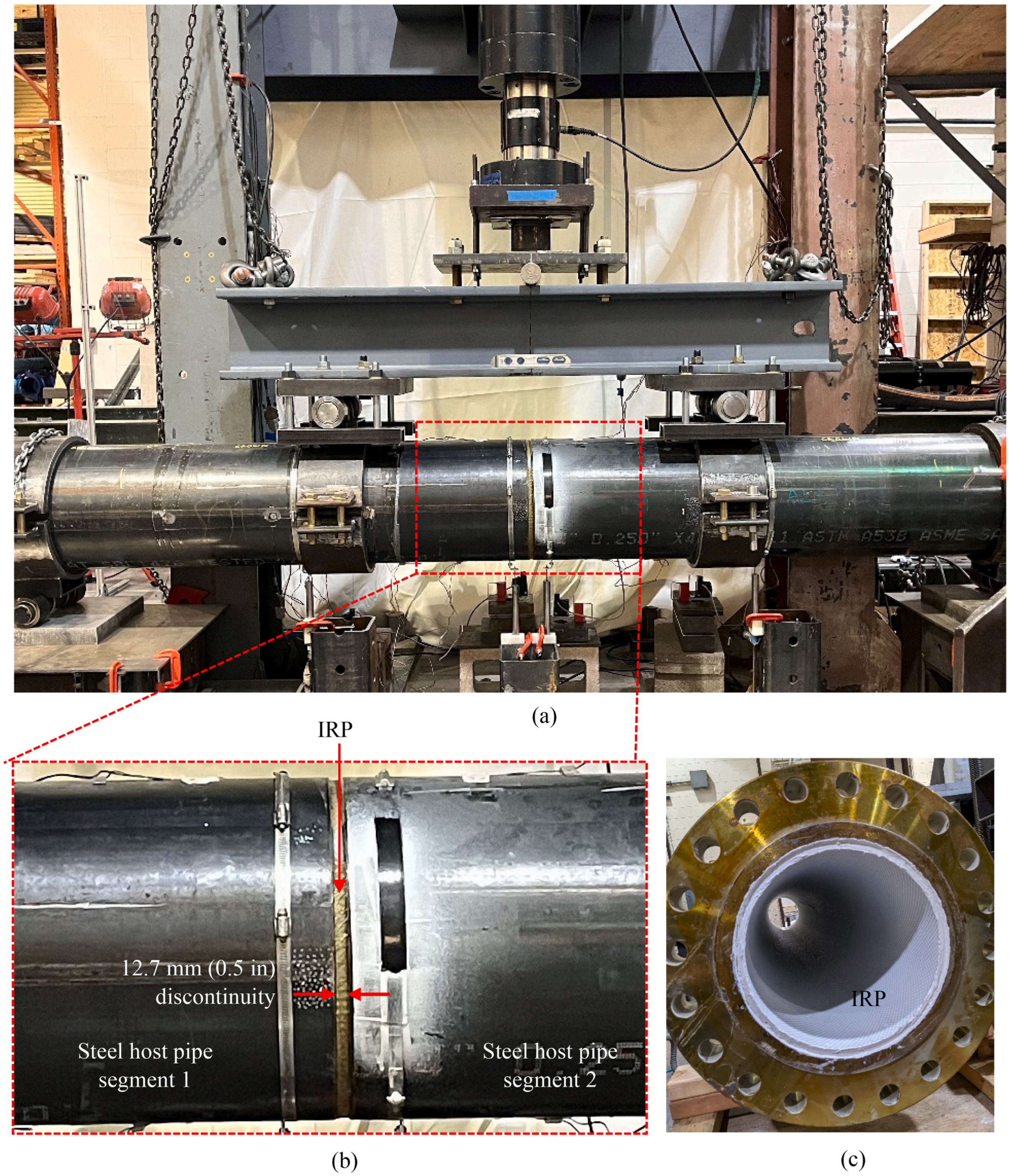

Fig. 1. (a) Actual experimental bending test setup of IRP installed in host pipe with a circumferential discontinuity at the midspan, (b) Longitudinal view of circumferential discontinuity and (c) Interior view of repaired steel pipe with IRP (CUB).

discontinuity width of the host pipe, thickness and MOE of the repair material, and level of loading on the bending fatigue performance of IRP-repaired discontinuous host pipe segments. Furthermore, the relative contribution of the investigated parameters to the critical stress and fatigue life of IRP in discontinuous host pipes during cyclic bending are also assessed using multiple regression analysis. The results of this study provide a detailed understanding of how key design parameters affect the fatigue behaviour of IRP systems, which enables their effective design, development, and field application.

2. Numerical modelling and analysis

2.1. Geometry, contact types and boundary conditions

Three-dimensional FE four-point bending simulations are carried out using ANSYS mechanical [55] to assess the fatigue performance of IRP systems under repetitive surface load from overhead traffic over 50 years of service life. These simulations are based on an experimental load configuration of 762–1016-762 mm (30–40-30 in) implemented at the University of Colorado Boulder (CUB), as illustrated in Fig. 1 and Fig. 2. The FE simulations include scenarios where the IRP is evaluated

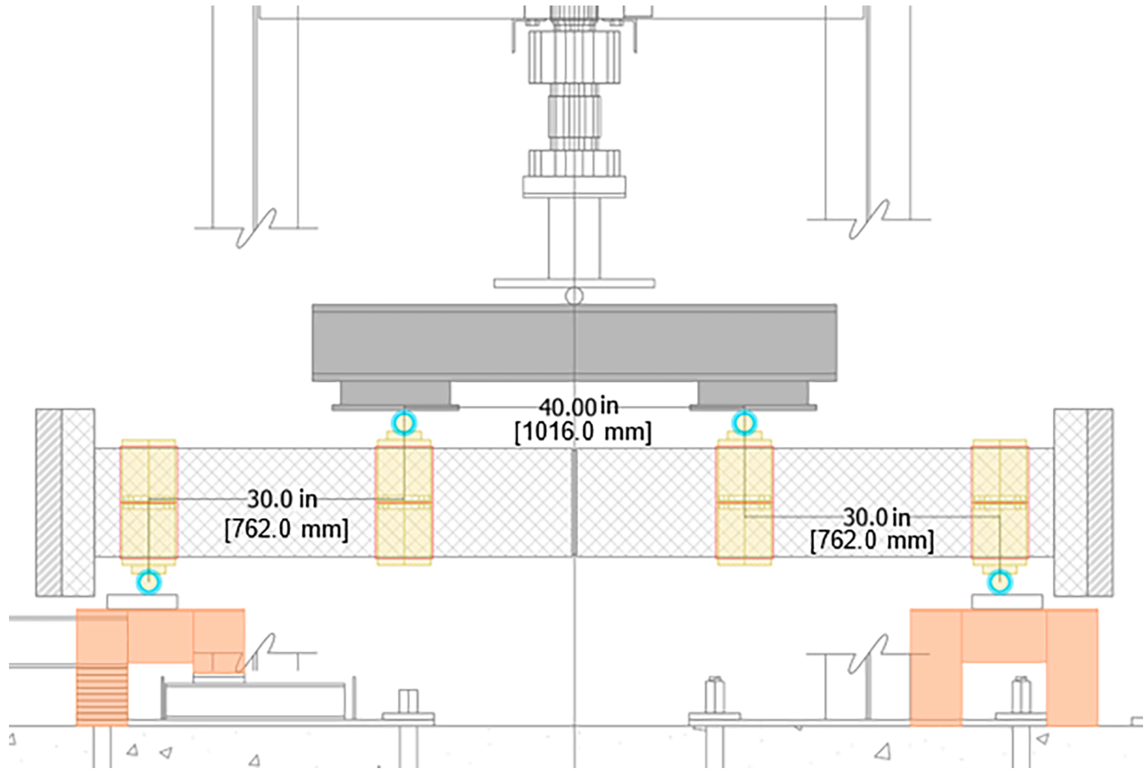

Fig. 2. Instrumentation schematic of bending test setup (CUB) [Units: in].

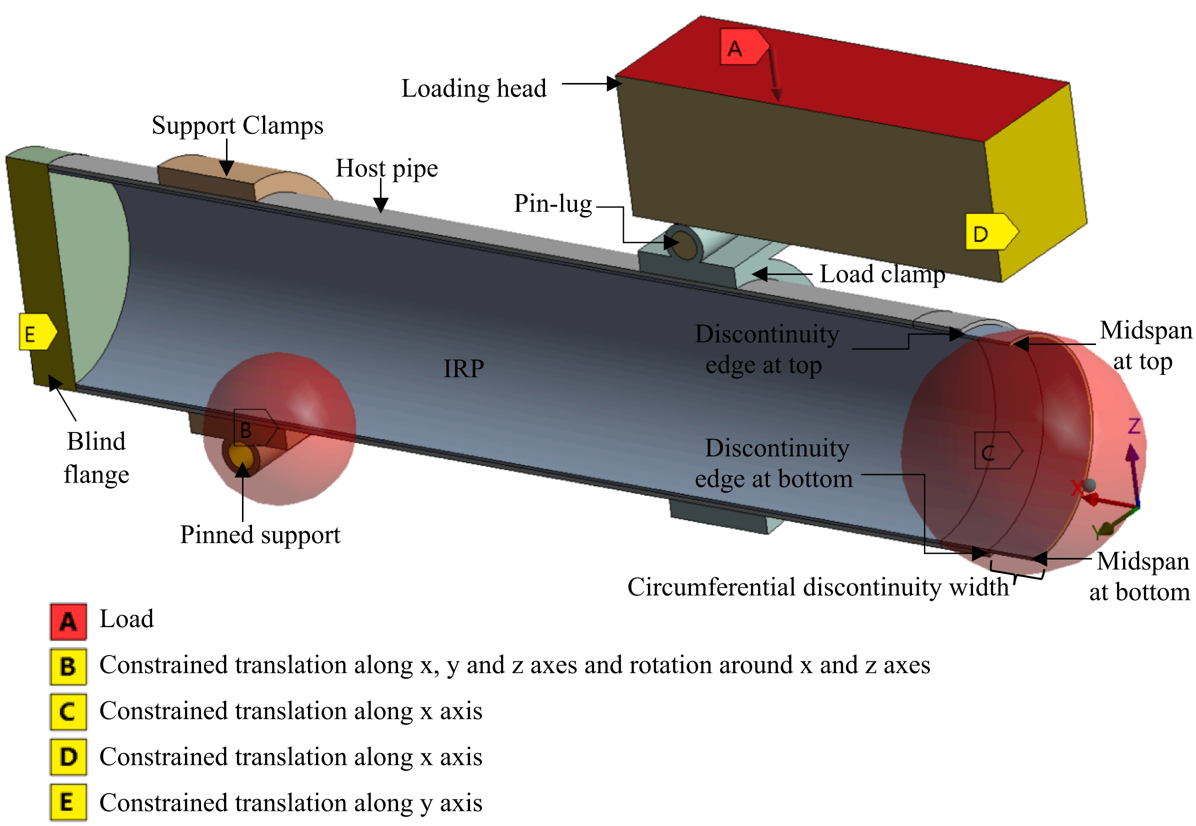

Fig. 3. (a) A quarter of the geometry of the FE model of an IRP installed in a host pipe with 152.4 mm (6 in) discontinuity at the midspan with loading and boundary conditions.

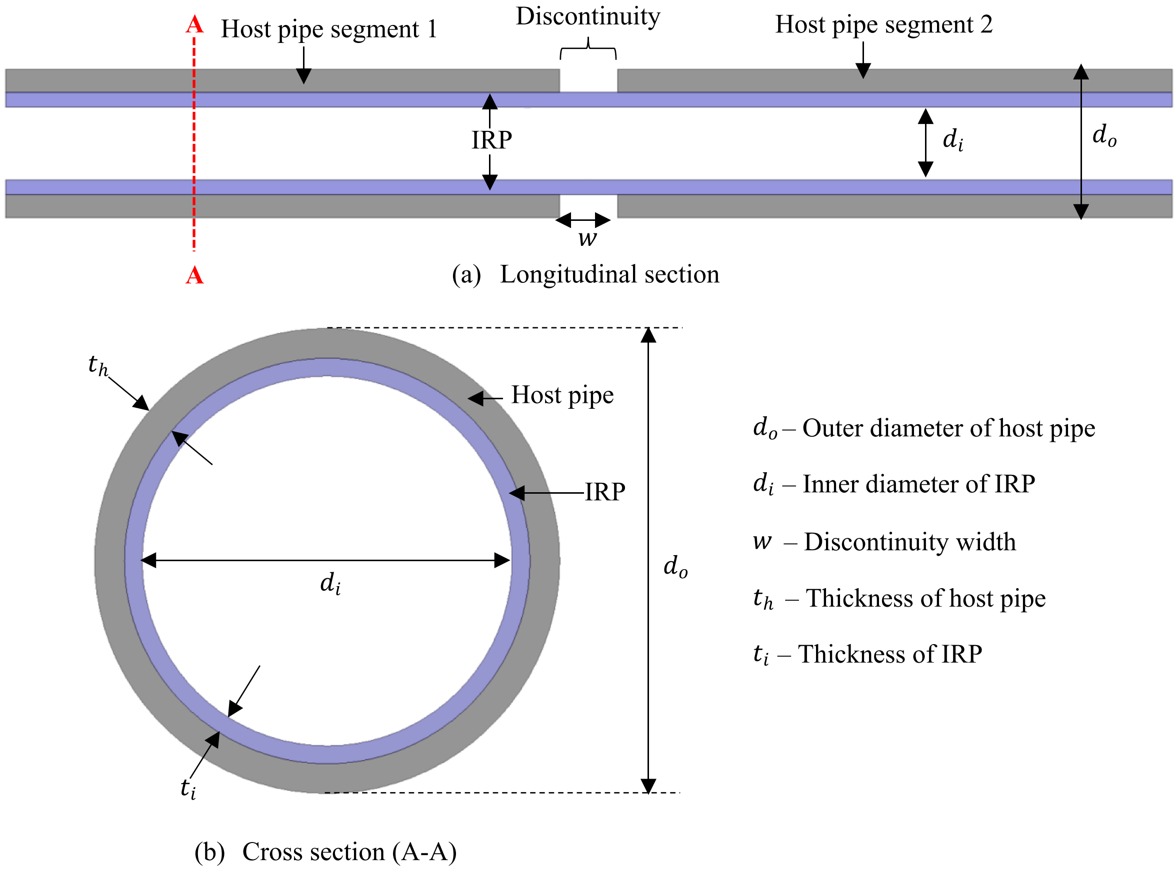

Fig. 4. Schematic diagram of IRP installed in discontinuous host pipe.

when it is alone, as well as when installed in a continuous (undamaged) host pipe and in a host pipe with a circumferential discontinuity at the midspan. To minimise computational time, only a quarter of the system is modelled considering symmetry, with appropriate boundary conditions applied (Fig. 3). Fig. 4 displays a schematic diagram of an IRP installed in a discontinuous host pipe. Throughout the investigation, the outer diameter and thickness of the host pipe are kept constant at 325.85 mm (12.83 in) and 6.35 mm (0.25 in), respectively [50]. The outer diameter of the IRP is defined by the inner diameter of the host pipe, which is 311.15 mm (12.25 in), and the thickness is assumed to be 4.115 mm (0.162 in). However, in the parametric study, the thickness of the IRP varies from 3.175 mm (0.125 in) to 9.525 mm (0.375 in). Further, the discontinuity widths of the host pipe considered are 12.7 mm (0.5 in), 25.4 mm (1 in), 50.8 mm (2 in), 101.6 mm (4 in), and 152.4 mm (6 in). The discontinuity width of 12.7 mm (0.5 in) reflects an axial pulled-out failure of a weak joint in a segmental legacy pipeline. This type of failure can be attributed to earthquake indued transient ground deformation and repetitive axial loading, which is typically induced by thermal expansion and contraction [22,56–58]. A discontinuity width of 152.4 mm (6 in) on the other hand indicates excessive deterioration of legacy pipelines caused by corrosion and ageing [10,59]. These parameters are selected based on a prior study conducted by Kiriella et al [50].

Table 1
Properties of IRP materials.

Material	MOE GPa	MOE ksi	Poisson's ratio	Reference
Polymer	1.744	253	0.11	Mellott and Fatemi [62]
Thermoplastic	2.762	401	0.11	Mellott and Fatemi [62]
ALTRA10	3.739	542	0.23	Laboratory testing
GFRP-1	7.9	1,146	0.25	Zakaria et al [63]
GFRP-2	14.03	2,035	0.25	Huh et al [64]
GFRP-3	26.43	3,833	0.25	Huh et al [64]
GFRP-4	38.63	5,603	0.25	Huh et al [64]
CI	70	10,153	0.29	Seica and Packer [65]
Steel	200	29,008	0.29	Preedawiphat et al [66]

To accurately simulate the mechanical contacts within the experimental test setup, while avoiding any convergence issues, a pinned support with frictionless connection between the outer surface of the host pipe and the support clamp is used. The loading head is connected to another clamp using a pin-lug system. Both clamps have an inner diameter that matches the outer diameter of the host pipe, and their thickness measures 25.7 mm (1.01 in). Frictionless connections are used between the pin-lug and load clamp, as well as between the load clamp and host pipe. Additionally, a blind flange is used to seal the open end of the quarter model of pipe. The thickness of the blind flange is 66.5 mm (2.62 in), and its diameter is equal to the outer diameter of the host pipe. In the FE model, it is assumed that the host pipe and the IRP are adhered to each other along their entire interface using the bonded connection type available in ANSYS Mechanical. This contact type does not allow sliding or separation between faces or edges. The normal and tangential forces are very strong exerting resistance against the forces that may induce relative motion between surfaces. Bonded contact facilitates a linear solution as the contact length/area remains unchanged throughout the load application process. The test involves subjecting the IRP system to 14.8 kN (3.3 kips) of vehicular traffic loading, as determined by Klingaman et al [21] utilising the procedure recommended by Petersen et al [60] for evaluating the live load distribution to buried concrete culverts. This level of loading, which is repeated 1 million times, is equivalent to the traffic load that an IRP system is anticipated to experience over a service life of 50 years. Additionally, the parametric study involves varying levels of surface loads to further examine the effect of the loading magnitude on the repair system.

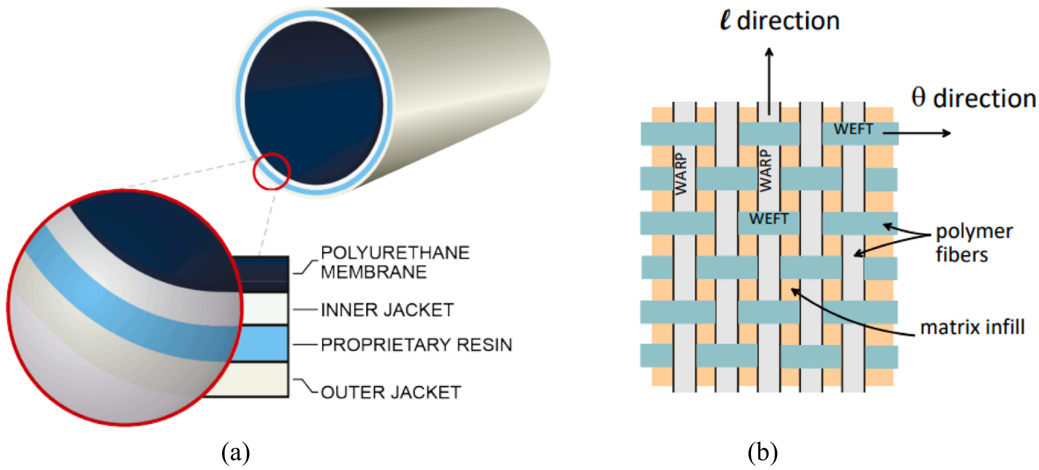

Fig. 5. Schematic of ALTRA10 (a) lining components and [68] warp and weft yarn pattern [67].

2.2. Element types and material properties

The entire system, which includes the IRP, host pipe, clamps and loading head, is modelled using the standard SOLID 186, a higher-order 3D solid element that comprises 20 nodes. Each node has three degrees of freedom, including movement in the x, y and z nodal directions and it also exhibits quadratic displacement behaviour. Additionally, the elements can undergo large deformation and strain, exhibit plasticity, display hyper-elasticity, experience stress stiffening and show creep behaviour [61]. Throughout the analysis, the host pipe is assigned as steel, whereas a variety of potential IRP materials are employed. As shown in Table 1, these IRP materials include polymers, composites and metallic materials. Additionally, steel is employed for all the remaining components of the setup, including clamps, lugs, pins, loading head and blind flange. It should be noted that if not specified, the IRP material used in the analyses is ALTRA10 structural lining supplied by Sanexen Environmental Services Inc. (Quebec, Canada). The analysis is carried out under the assumption of two design strain limits of the IRP material systems, which are 0.02 for polymeric and composites systems (MOE of 38.63 GPa/ 5,603 ksi or less) and 0.002 for metallic systems (MOE of 70 GPa/ 10,1523 ksi or greater). These design strain limits are based on the work of Tafsirojjaman et al [17].

Further information regarding the composition of the aforementioned IRP materials is provided below.

- Polymer – The material under consideration is a pure, unreinforced (neat) form of an impact polypropylene copolymer [62].
- Thermoplastic – The material under investigation is a blend of polypropylene and thermoplastic elastomers. The elastomer component constitutes approximately 25 % of the total weight of the material and contributes to its elasticity [62].
- ALTRA10 – This is formerly known as Aqua-Pipe® which is a commercial lining material developed by Sanexen Environmental Services Inc. (Quebec, Canada). This material is employed in the production of CIPP liners for rehabilitating water mains. As shown in Fig. 5a, ALTRA10 is an epoxy resin-impregnated lining consisting of an inner and outer layer each composed of seamless, circular woven fabric. Each layer of woven fabric consists of polyethylene thermoplastic yarn in the longitudinal (warp) direction and in the circumferential (weft) direction, as shown in the schematic in Fig. 5b. Comprehensive details regarding this lining material can be found in the publications by O'Rourke et al [67] and Matthews et al [68].

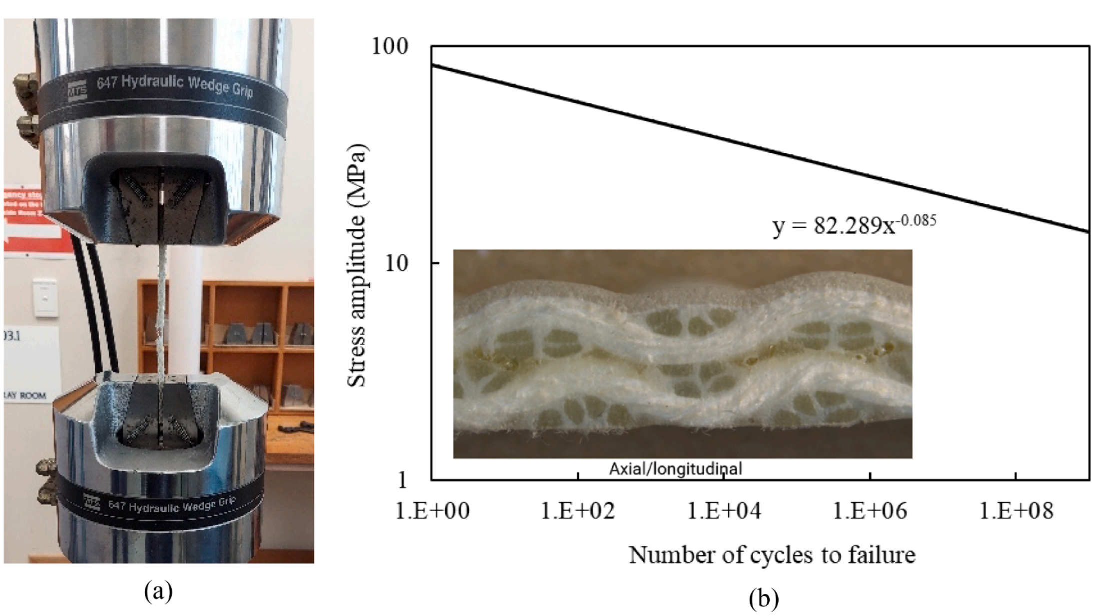

Fig. 6. (a) Tension-tension fatigue test (b) Stress-Life (S-N) curve of ALTRA10 IRP material (with mean stress correction).

Table 2
References that include S-N curves for IRP materials, along with their corresponding stress ratios.

Material	Stress ratio	Reference
Polymer	−1	Mellott and Fatemi [62]
Thermoplastic	−1	Mellott and Fatemi [62]
ALTRA10	0.1	Laboratory testing
GFRP-1	0.1	Zakaria et al [63]
GFRP-2	0.1	Huh et al [64]
GFRP-3	0.1	Huh et al [64]
GFRP-4	0.1	Huh et al [64]
CI	−1	Rausch et al [74]
Steel	−1	Gorash and MacKenzie [75]

- GFRP 1 – The composition of this material consists of unidirectional E-glass fibre and epoxy resin. The fibre orientation is 0/90° [63].
- GFRP 2 – This material is composed of E-glass fibre and epoxy resin, with a fibre orientation of ± 45° (Bidiagonal glass fibre) [64].
- GFRP 3 – This material is fabricated from E-glass fibre and epoxy resin. The fibres are oriented at an angle of 0 ± 45°, forming a triaxial glass fabric [64].
- GFRP 4 – This is a composite material made from E-glass fibre and epoxy resin. The fibres are oriented in a unidirectional manner, with a 0° angle[64].
- CI – The investigation employs a CI of ENGJL-270 grade, a type of cast iron that contains lamellar graphite, commonly referred to as grey iron [65].
- Steel – The type of structural steel utilised in this study is ASTM A36 [66].

2.3. Stress-life approach

There are three fundamental approaches for conducting fatigue analysis, including the stress-life approach, the strain-life method, and the crack growth method [69]. Considering that the projected design life for this investigation is one million cycles, the stress-life approach is utilized. This method is particularly appropriate for scenarios involving high-cycle fatigue, where materials experience cyclic loading primarily within their elastic range [70]. The stress-life approach is based on fatigue data represented by an S-N curve, which is derived from laboratory testing and does not account for crack initiation or growth [71]. By assuming a correlation between stress and expected fatigue life, the stress-life method calculates the life span of a structure or structural component based on its stress history and the S-N curve [72]. In the present study, the S-N curve of ALTRA10 repair material was established by performing laboratory tensile-tension fatigue testing in accordance with ASTM D 3479/D 3479 M [73], as shown in Fig. 6. The stress-life data for polymeric, thermoplastic, GFRP and metallic IRP materials were obtained from previously published journal papers, which are referenced in Table 2. The stress ratios (R) applied during the fatigue testing of these materials can also be found in Table 2.

The stress-life approach starts with calculating the stress values of the components of IRP under static loading. The study focuses on normal stress in the longitudinal direction (x-axis), as it is the dominant stress type during bending. The simulation of the fatigue resulting from cyclic loading is then performed using the fatigue tool, which calculates the effective alternating stress based on the magnitude of the maximum and minimum stresses. The amount of damage resulting from a stress cycle is influenced by the alternating stress and the mean stress [71,76]. As a result, the level of mean stress during a stress cycle is significant for the stress-life approach. In this study, the loading cycle being examined is

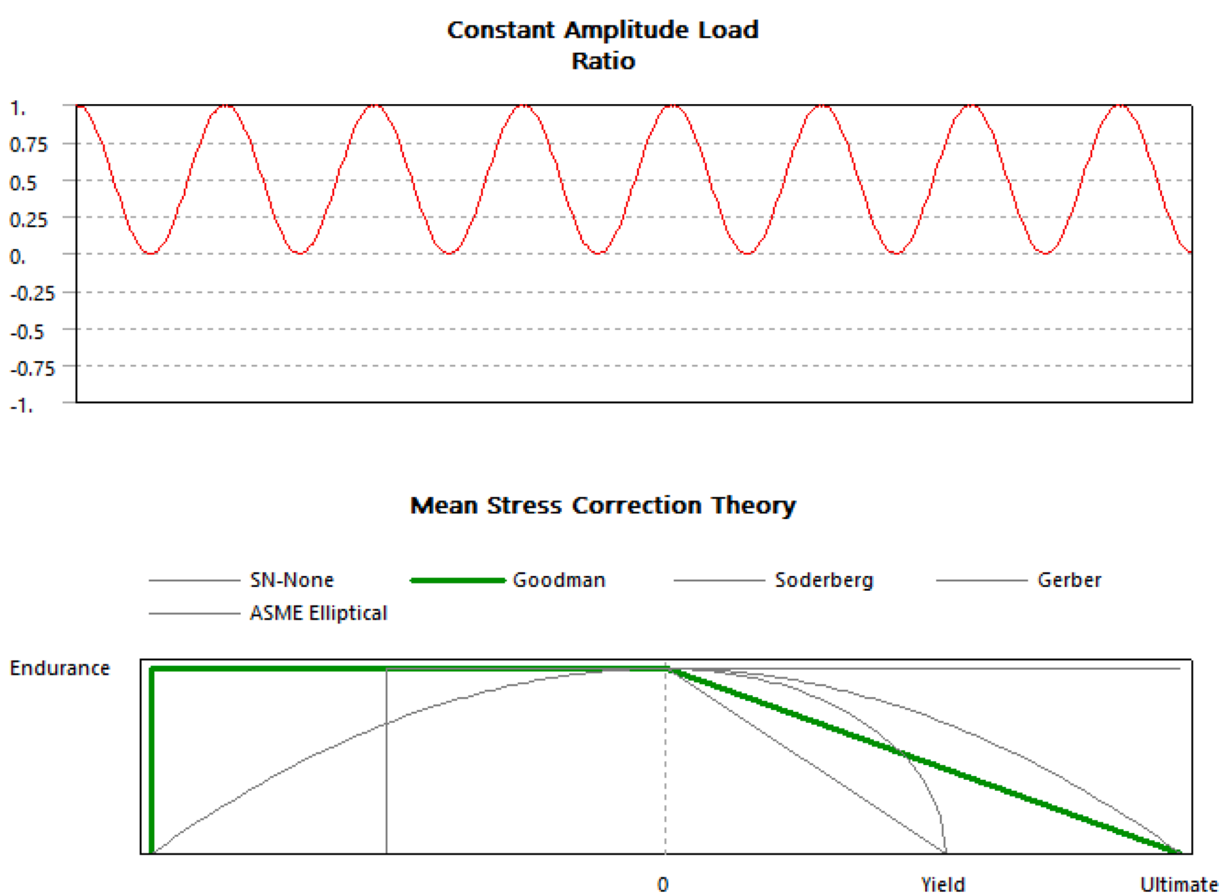

Fig. 7. Constant amplitude load ratio and mean stress correction theory applied in bending fatigue simulations.

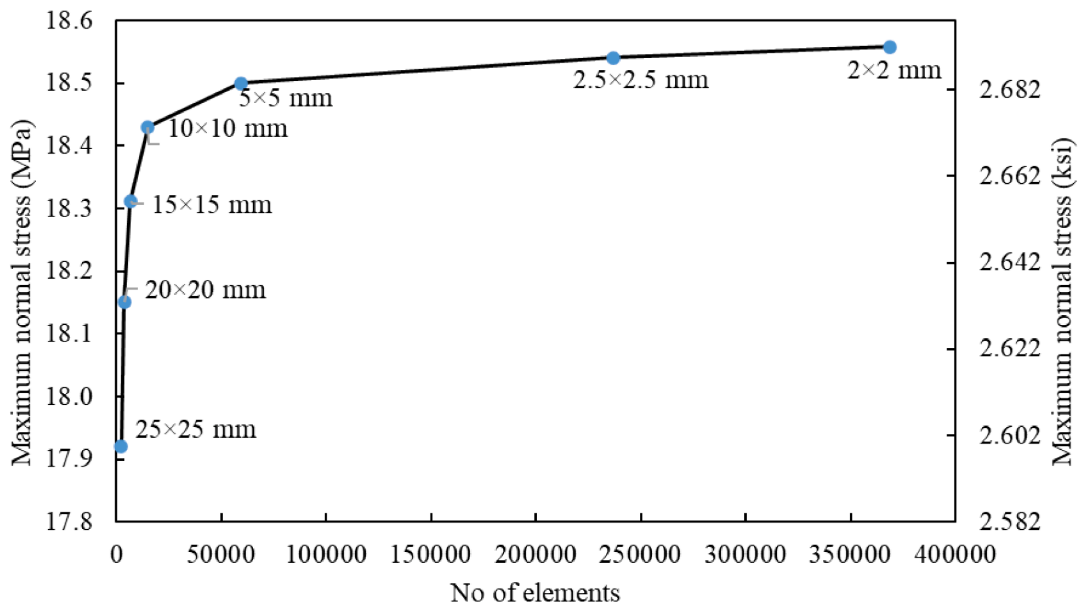

Fig. 8. Mesh convergence.

conducted under nonzero mean stress, and thus, the mean stress that arises is adjusted using a mean stress correction theory (Fig. 7). The Goodman mean stress theory (Eq. (1)) is applied to convert the applied stress cycle into an equivalent stress cycle with zero mean stress [36,71,77–80]. The corrected alternating stress (effective alternating stress) is then projected onto the S-N curve of the material to define the alternating stress at the failure and determine the corresponding life cycles.

$$\frac{S_a}{S_e} + \frac{S_m}{S_u} = 1 \tag{1}$$

where S_a is the stress amplitude or alternating stress given by Eq.(2), S_e is the corrected alternating stress or effective alternating stress, S_m is the mean stress given by Eq.(3) and S_u is the ultimate tensile strength

$$S_a = \frac{S_{max} - S_{min}}{2} \tag{2}$$

$$S_m = \frac{S_{max} + S_{min}}{2} \tag{3}$$

where S_{max} is the maximum stress and S_{min} is the minimum stress.

2.4. Mesh convergence study and mesh refinement

A mesh convergence study is conducted to identify the optimal mesh size for producing reliable FEA results. The accuracy of numerical solutions is assessed by comparing the maximum normal stress generated by FEA with the maximum theoretical stress of 18.8 MPa (2.72 ksi) calculated using the bending stress formula (Eq. (4)) This is done by simulating an IRP pipe with a MOE of 3.739 GPa (542 ksi) under a traffic

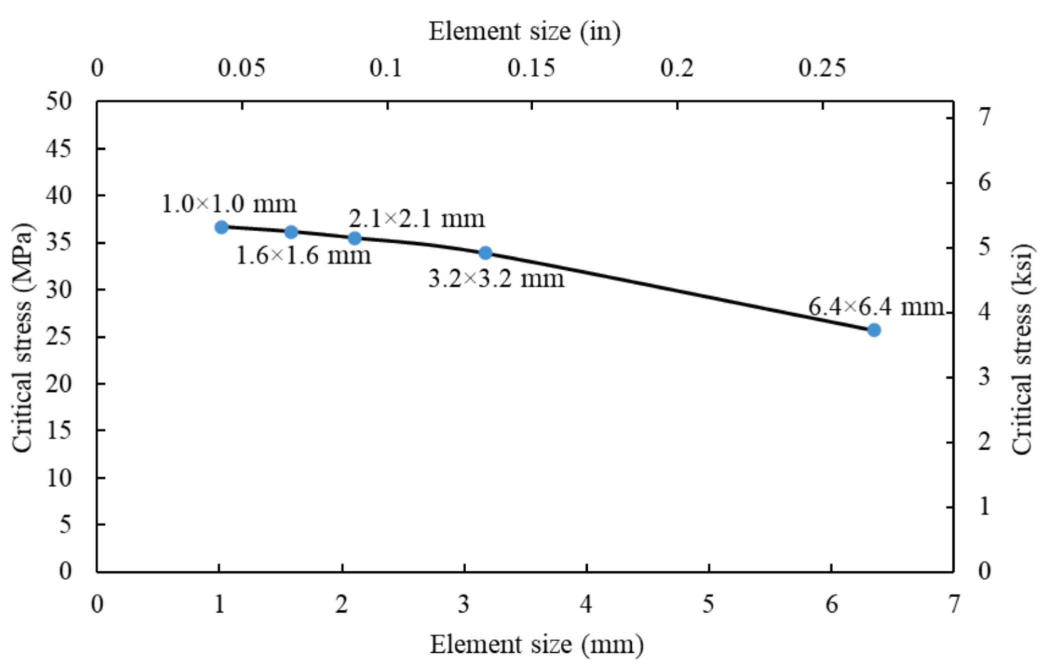

Fig. 9. Mesh sensitivity study for critical stress in refinement region.

Table 3
Number of elements in the compound section of host pipe and IRP with different discontinuity widths after mesh refinement.

Width of host pipe discontinuity		Number of elements in the compound section of the host pipe and IRP
mm	in	
12.7	0.5	209,061
25.4	1	208,761
50.8	2	207,861
101.6	4	206,361
152.4	6	204,861

loading of 14.8 kN (3.3 kips). The pipe used in the mesh convergence study has the same dimensions as the IRP outlined in section 2.1. The mesh size in the direction of thickness is set to three elements, and the surface element size of the pipe varies from coarse (25 × 25 mm or 0.984 × 0.984 in) to very fine (2 × 2 mm or 0.079 × 0.079 in). Fig. 8 displays the relationship between the maximum normal stress and the number of elements in the mesh of FEA models. The figure indicates that the accuracy of the FEA solution is within 1.6 % of the theoretical result when an element size of 5 × 5 mm (0.197 × 0.197 in) or smaller is employed.

$$\sigma = \frac{M}{S} \tag{4}$$

where σ is the bending stress, M is the bending moment, S is the section modulus of IRP.

A mesh sensitivity analysis was performed in order to determine the optimal surface element size for refining the mesh in the vicinity of the discontinuity edge of the host pipe, with the aim of accurately capturing potential stress concentrations (Fig. 9). For this, a steel host pipe with a 12.7 mm (0.5 in) wide discontinuity repaired using the same IRP that was employed for the mesh convergence discussed above is analyzed under traffic loading of 14.8 kN (3.3 kips). Taking into account the computational efficiency, the mesh is refined along a length equal to the width of the host pipe discontinuity and an additional 76.2 mm (3 in) beyond the edge of discontinuity. In sensitivity analysis, the surface

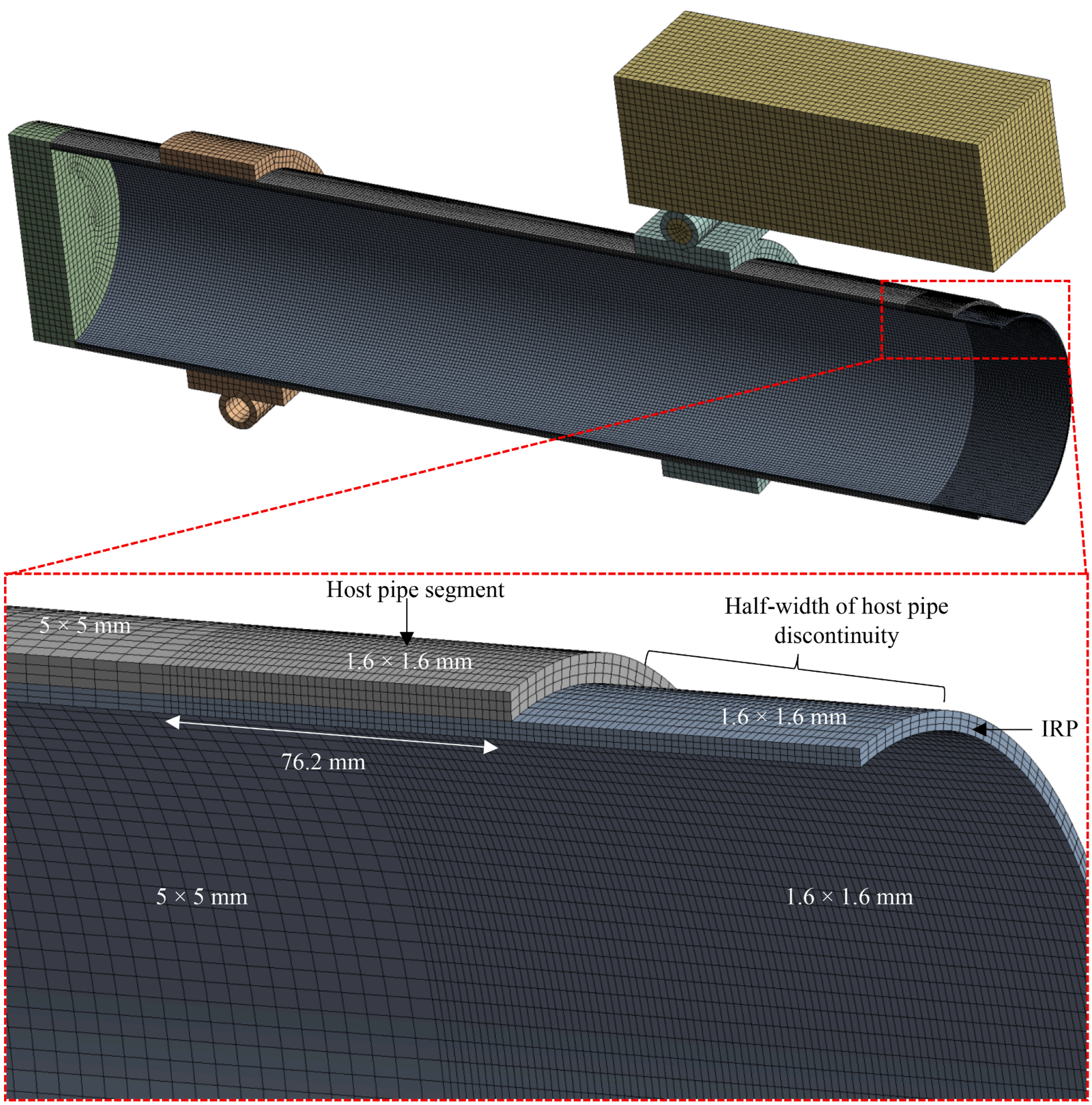

Fig. 10. Mesh refinement of quarter FE model of an IRP installed in host pipe with 152.4 mm (6 in) wide discontinuity.

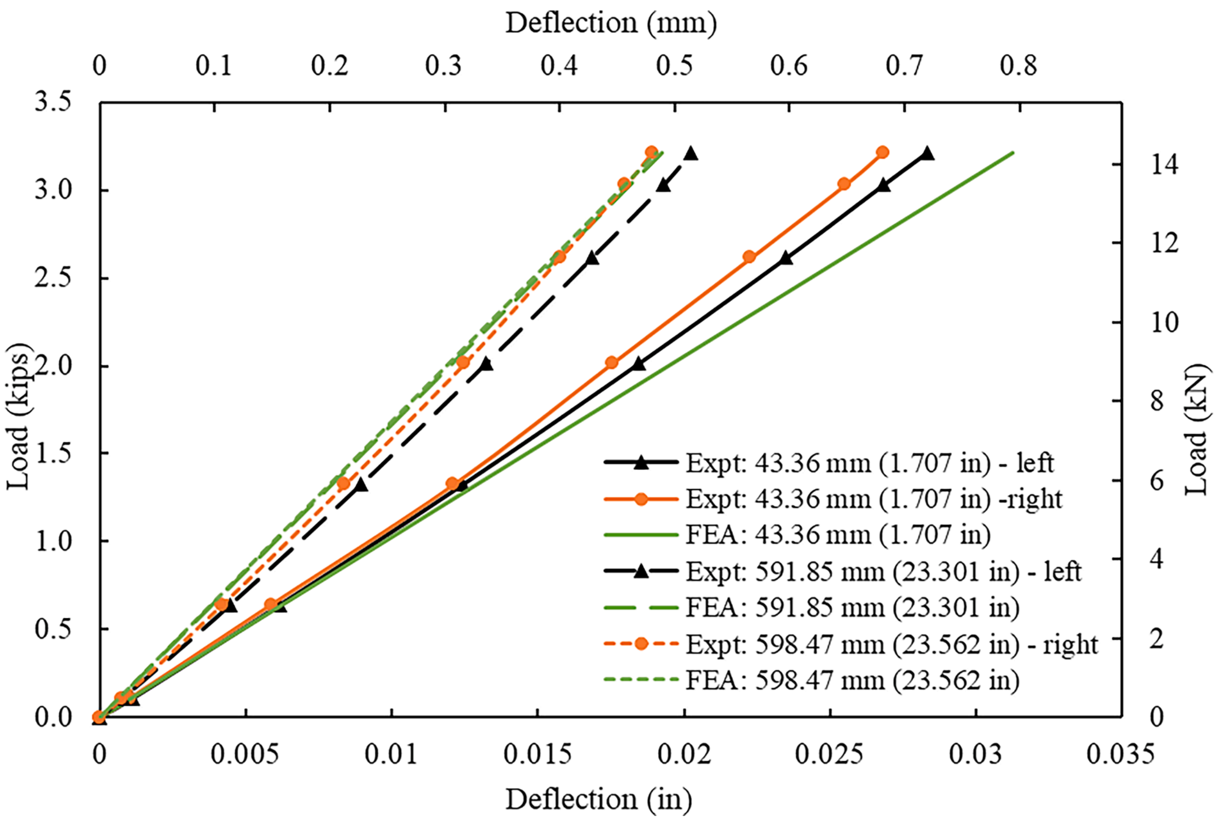

Fig. 11. Comparison between FEA and experimental load–deflection behaviours.

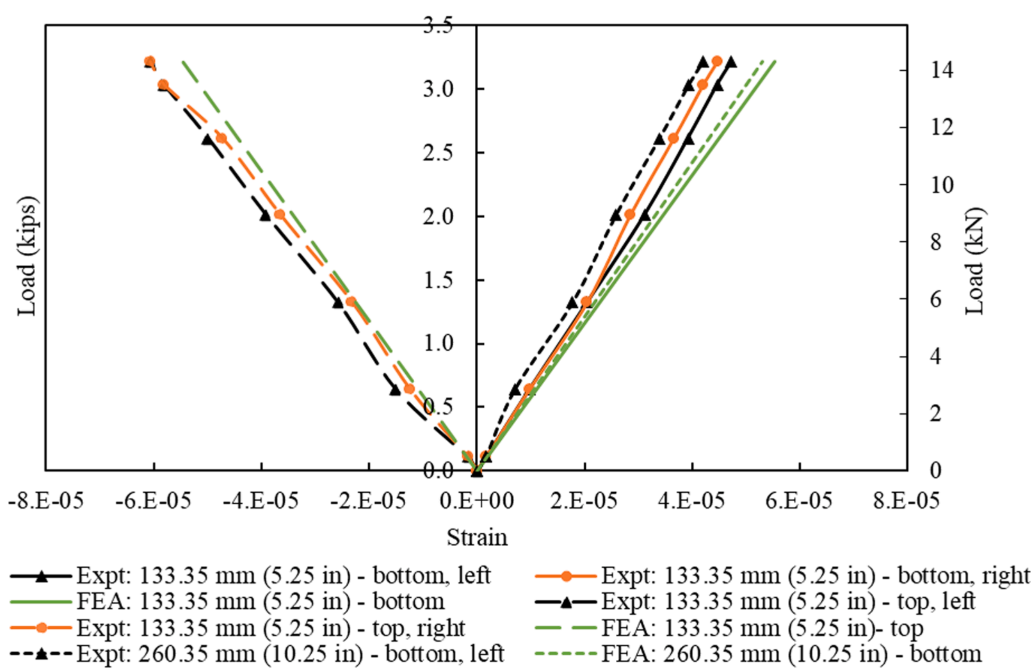

Fig. 12. Comparison between FEA and experimental load - strain behaviours.

element sizes of refined mesh are varied between 6.4 × 6.4 mm (0.252 × 0.252 in) and 1.0 mm × 1.0 mm (0.039 × 0.039 in). In areas outside of these refined regions, a 5 × 5 mm (0.197 × 0.197 in) element size is used. Fig. 9 illustrates the influence of different element sizes used for mesh refinement on the localized stress in the IRP at the edge of host pipe discontinuity. Accordingly, localized stress at the discontinuity edge begins to converge towards a finite value when a surface element size of less than 2.1 × 2.1 mm (0.083 × 0.083 in) is used. After considering the computational cost and the observation that the discrepancy in the local stress at the discontinuity edge between element sizes of 1.0 mm × 1.0 mm (0.039 × 0.039 in) and 1.6 × 1.6 mm (0.063 × 0.063 in) is within 2.0 %, it has been decided to select an element size of a 1.6 × 1.6 mm (0.063 × 0.063 in) for refining mesh. The selected element size is applied for refining the mesh across systems with varying

Table 4
Discrepancies in the maximum deformations observed between experimental data and FEA.

Location	Expt mm	in	FEA mm	in	Difference (%)
43.36 mm (1.707 in) from the midspan on the left-side section	7.19E-01	2.83E-02	7.94E-01	3.12E-02	9.4
43.36 mm (1.707 in) from the midspan on the right-side section	6.81E-01	2.68E-02	7.94E-01	3.12E-02	14.2
591.85 mm (23.301 in) from the midspan on the left-side section	5.14E-01	2.02E-02	4.89E-01	1.92E-02	4.9
598.47 mm (23.562 in) from the midspan on the right-side section	4.80E-01	1.89E-02	4.84E-01	1.91E-02	0.9

Table 5
Discrepancies in the maximum strains observed between experimental data and FEA.

Location	Expt mm	in	FEA mm	in	Difference (%)
133.35 mm (5.25 in) distance from the midspan at the bottom of the left-side section	1.20E-03	4.73E-05	1.41E-03	5.53E-05	14.5
133.35 mm (5.25 in) distance from the midspan at the bottom of the right-side section	1.13E-03	4.46E-05	1.41E-03	5.53E-05	19.3
133.35 mm (5.25 in) distance from the midspan at the top of the left-side section	−1.54E-03	−6.07E-05	−1.39E-03	−5.46E-05	10.1
133.35 mm (5.25 in) distance from the midspan at the top of the right-side section	−1.54E-03	−6.07E-05	−1.39E-03	−5.46E-05	10.1
260.35 mm (10.25 in) distance from the midspan at the bottom of the left-side section	1.07E-03	4.19E-05	1.35E-03	5.30E-05	20.9

discontinuity widths. Table 3 presents the total number of elements found in the compound section of the host pipe and IRP after mesh refinement. The mesh refinement of a quarter symmetry model of an IRP installed in a host with 152.4 mm (6 in) wide discontinuity is shown in Fig. 10.

2.5. Validation of the FE model

The FEA results are validated using the outcomes from a laboratory experiment conducted by CUB to ensure the accuracy of the model. This involves comparing the FE and experimental load–deflection (Fig. 11), and load–strain (Fig. 12) behaviours at different locations at the bottom (tension side) and top (compression side) of an ALTRA10 IRP in a steel host pipe with a discontinuity width of 12.7 mm (0.5 in) under a traffic load of 14.3 kN (3.2 kips). Fig. 11 demonstrates a good correlation between FEA and experimental load–deflection behaviours, with a maximum deviation of 14.2 % at 43.36 mm (1.707 in) from the midspan on the right-side section (Table 4). (It should be noted that the absence of a strain gauge at the midspan is due to the difficulty encountered during installation, primarily resulting from the limited width of discontinuity). As shown in Fig. 12, the FEA load–strain behaviour agrees well with the corresponding experimental results, with maximum variations of 20.8 % at 260.35 mm (10.25 in) distance from the midspan at the bottom of the left-side section (Table 5).

2.6. Hot-spot stress for calculating stress concentration

Hot-spot stress (HSS) is widely recognized as an appropriate measure for the maximum stress at a discontinuity of a segment, which can be applicable for fatigue analysis of IRP systems installed in host pipes with discontinuities. To determine HSS, it is necessary to compute the surface stress field in the immediate vicinity of the edge of the discontinuity [81]. Extrapolation procedures are then applied to specific pre-defined stress evaluation points to obtain HSS [82]. Based on the study conducted by Haghpanahi and Pirali [83], which focuses on acrylic tubular joints without weld fillet, as well as the extrapolation rules proposed by the international institute of welding (IIW), it has been selected that the initial extrapolation point should be positioned at a distance of 0.4 times the thickness of IRP from the edge of discontinuity and the second point is chosen to be located 0.6 times the thickness of IRP beyond the first point [84]. The HSS is determined by performing a linear extrapolation of the geometric stress at these two specified points to the edge of discontinuity. The process is illustrated in Fig. 13 and can be mathematically represented by Eq. (5).

where t_i is the thickness of IRP, σ_{hs} is the HSS, $\sigma_{0.4t_i}$ is the stress at a distance of 0.4 times the thickness of IRP from the edge of discontinuity and $\sigma_{1.0t_i}$ is the stress at a distance of 0.6 times the thickness of IRP beyond the first point.

$$\sigma_{hs} = 1.67\sigma_{0.4t_i} - 0.67\sigma_{1.0t_i} \tag{5}$$

Fig. 14 shows a comparison between the HSS and localized FE stress in the tension side of IRP at the edge of host pipe discontinuity. According to this figure, the HSS and the localized stress at the discontinuity edge follow a similar trend as the discontinuity width increases. It has been observed that the maximum difference between the HSS and the localized FE stress is less than 10 %, which is considered insignificant for this type of problem. While determining fatigue life using the HSS approach is not very time-consuming when analyzing a limited number of cases, it becomes more complex and time-consuming when dealing with a large number of different scenarios in parametric studies. This is because the use of the HSS approach requires manual calculation of the effective alternating stress and the corresponding fatigue life. Alternatively, by utilizing the local stress approach, the ANSYS fatigue tool can provide a direct measurement of the fatigue life, eliminating the need for manual calculations. Although local stress may be slightly over-conservative (within 10 % of HSS), it can still be considered a reasonable estimate. Consequently, the local stress approach is selected over the HSS approach for fatigue analysis of this study as it balances practicality with accuracy, efficiently fulfilling the analysis requirements.

3. Results and discussion

3.1. Effect of discontinuity width

The stress distribution over the length from the loading point to the midspan at the top (compression side) and bottom of IRP (tension side) in the presence of host pipe having a discontinuity width of 12.7 mm (0.5 in) under traffic load of 14.8 kN (3.3 kips) is compared in Fig. 15. The results indicate that a significant stress concentration arises at the edge of circumferential discontinuity at both the top and bottom of the IRP due to the abrupt change in cross-section caused by the presence of damaged host pipe segments (Fig. 16). This stress concentration decreases nonlinearly from the discontinuity edge to the midspan. The stress developed at the discontinuity edge at the tension side and compression side is 24.5 % and 16.3 % higher, respectively, than the

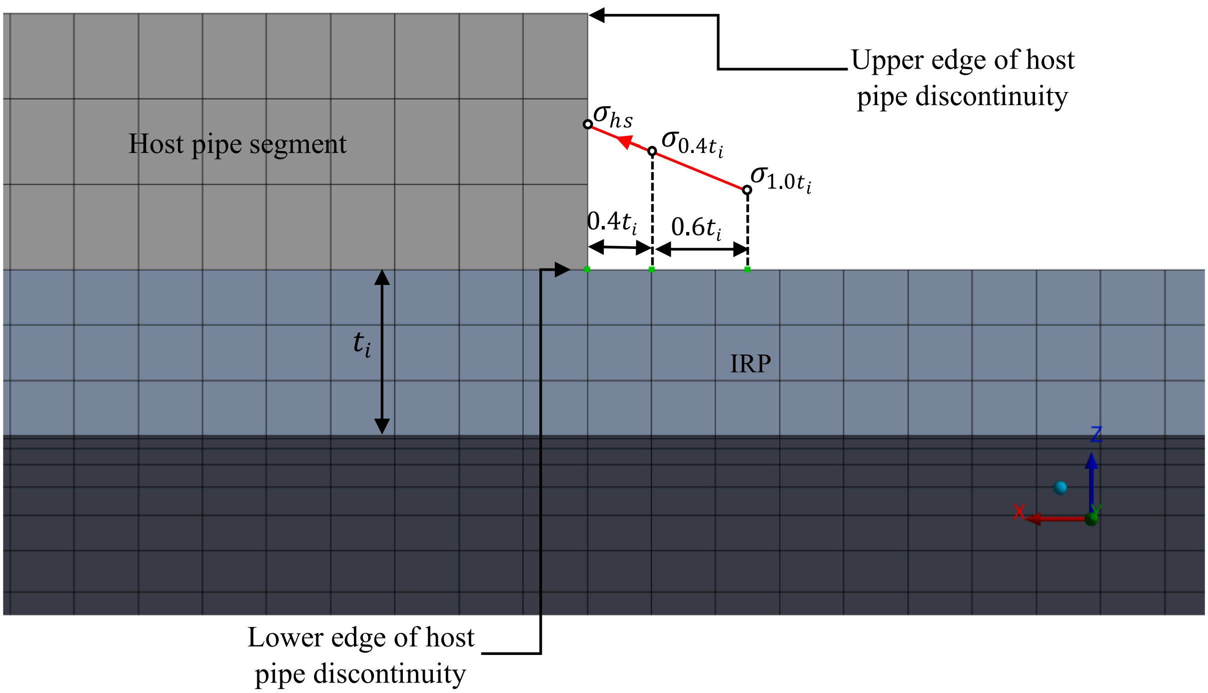

Fig. 13. Extraction of HSS from FE model using the linear extrapolation method.

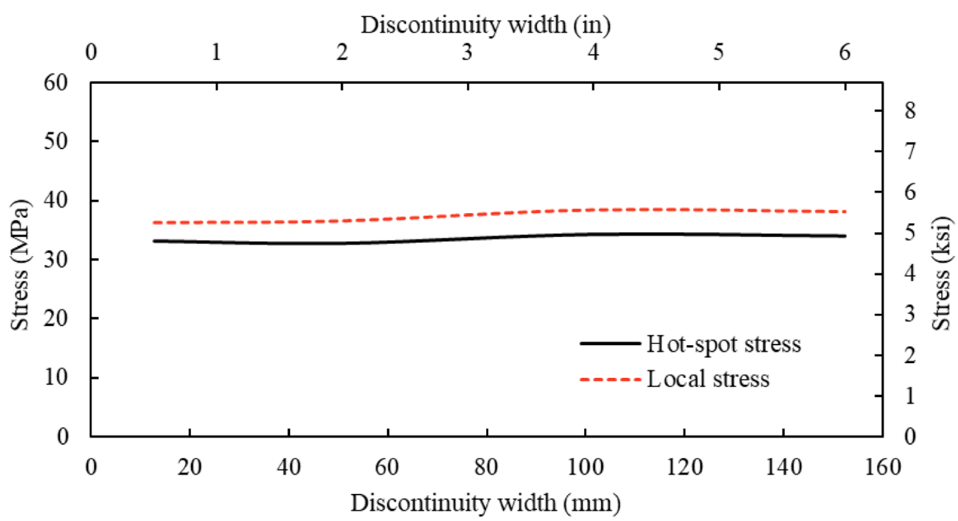

Fig. 14. Comparison of HSS and localized FE stress in the tension side of IRP at the edge of host pipe discontinuity.

stress developed at the midspan at the tension side and compression (Fig. 17). Note that in order to facilitate clear visualisation of stress distribution of IRP in the region of host pipe discontinuity, the host pipe segments have been temporarily hidden in Fig. 17. It can also be observed that the stress at the discontinuity edge at the crown of IRP is 5.6 % lower than that at the bottom. This observation highlights that stress concentration is much higher at the discontinuity edge at the bottom of IRP and can potentially control their fatigue failure/minimum fatigue life. It is desirable therefore to minimise stress concentration to prevent premature fatigue failure under cyclic bending when designing an IRP system for a host pipe with such discontinuities. According to Tien et al [18], the stress concentration issue could be addressed by introducing an appropriate unbonded length at the discontinuity edges. When subjected to bending, the unbonded length may allow the portion of the IRP that is not attached to the host pipe to move relative to the host pipe, thereby reducing stress concentration and extending fatigue life compared to the fully bonded condition.

The fatigue life contour plot of IRP around the midspan is shown in Fig. 18. Table 6 provides a summary of the fatigue life cycles at different locations of IRP. Based on the observations, it is evident that this IRP system has a minimum lifespan exceeding one million cycles. This suggests that even if the discontinuity edges of the host pipe segments cause stress concentration in IRP, the system will not fail before reaching its intended design life. This demonstrates that a thickness of 4.115 mm (0.162 in) and MOE of 3.739 GPa (542 ksi) are sufficient to safely withstand repeated traffic loads of 14.8 kN (3.3 kips) exerted for one million cycles of design fatigue life. In Fig. 19, the percentage of stiffness retained by ALTRA10 repair material is shown against the number of loading cycles at the three different applied alternating stress levels during the laboratory tension–tension fatigue tests of coupons. By extrapolating (linear) this dataset, considering a design life of 1 million cyles and maximum alternating stress obtained through FEA, it is

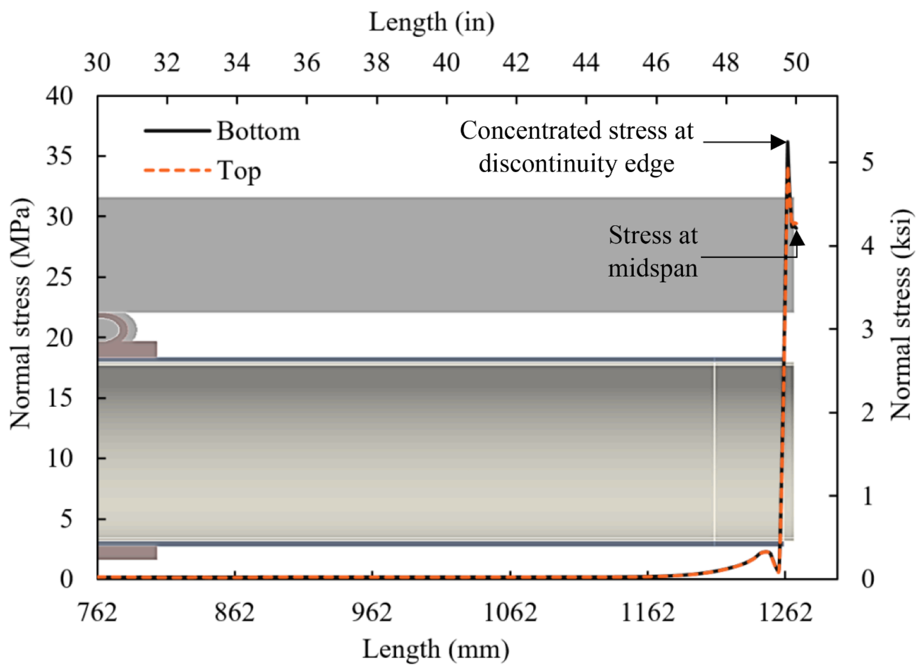

Fig. 15. Stress along the top (compression side) and bottom (tension side) of IRP from loading point to midspan.

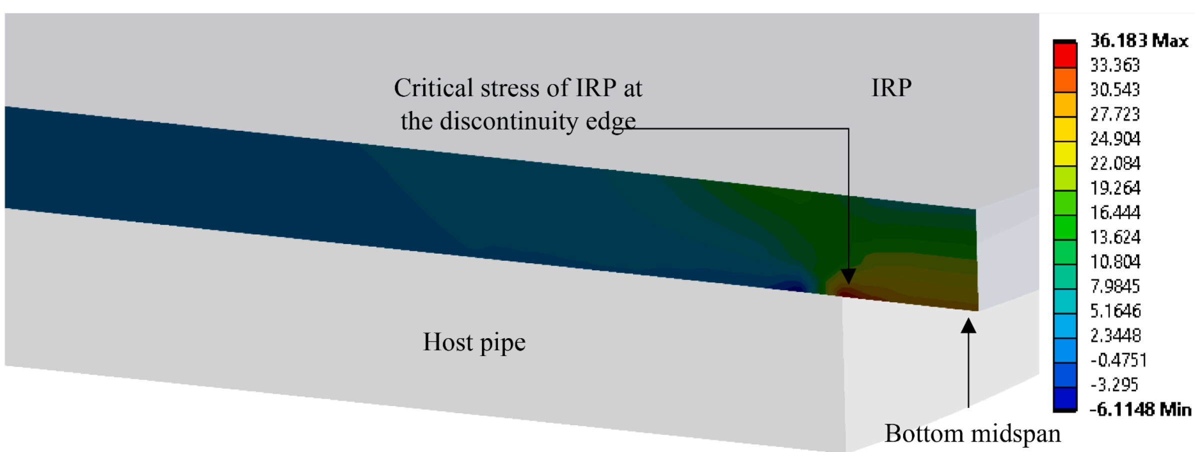

Fig. 16. Normal stress distribution along the x-axis at the bottom of IRP [units: MPa].

evident that even if the repair system would not fail at the design life under the imposed traffic load, its stiffness will degrade by 38.8 %. This finding is consistent with prior research [22,23], which demonstrated that while the CIPP repair system did not fail, stiffness loss could be observed under repetitive traffic loadings. However, this reduction in stiffness is significantly impacted by the stress concentration at the discontinuity edge.

Fig. 20 compares the stress in IRP at the midspan and at the edge of the host pipe discontinuity for different discontinuity widths, including zero (continuous host pipe), 12.7 mm (0.5 in), 25.4 mm (1 in), 50.8 mm (2 in), 101.6 mm (4 in), 152.4 mm (6 in) under the traffic load. Accordingly, when there is no damage in the host pipe, the maximum stress in the IRP is only 0.2 MPa (0.03 ksi) and is developed at the bottom midspan. This maximum stress is 98.1 % lower than the highest stress of the overall undamaged system, which occurs at the bottom midspan of the host pipe (Fig. 21a and b). This means that the presence of the continuous host pipe can stabilise the stresses generated in the IRP under repetitive lateral loading. Moreover, the minimum fatigue life of this IRP in a continuous host pipe system exceeds one billion cycles. When compared to the maximum stress that develops in an IRP installed in a continuous host pipe, the critical stresses generated in IRPs at the edges of host pipe discontinuities are 176.2 times higher. This demonstrates that while the continuous portion of the host pipe stabilises the stresses that develop in the IRP, the circumferential discontinuity induces the stress concentration in the repair pipe, potentially leading to fatigue failure. However, the stress concentration at the discontinuity edge, which controls the minimum fatigue life of the IRP in damaged host pipe systems, is almost the same for all discontinuity widths, with a maximum deviation of 5.0 %. The result indicates that the stress concentration in IRP at the discontinuity edge is independent of the width of the discontinuity. This is because, regardless of the discontinuity widths, the reduction in cross-sectional area at the discontinuity edge remains constant. Therefore, irrespective of the width of the host pipe discontinuity, when the same internal force is transmitted across the cross-sectional area at the discontinuity edge, the stress flow lines become denser (Fig. 22) by the same amount, resulting in constant stress amplification. Due to this, fatigue failure of IRP in fully bonded IRP systems with different discontinuity widths might occur at almost the same service life (Fig. 23). Under the imposed traffic load in the current study, the IRP systems for all discontinuity widths investigated will

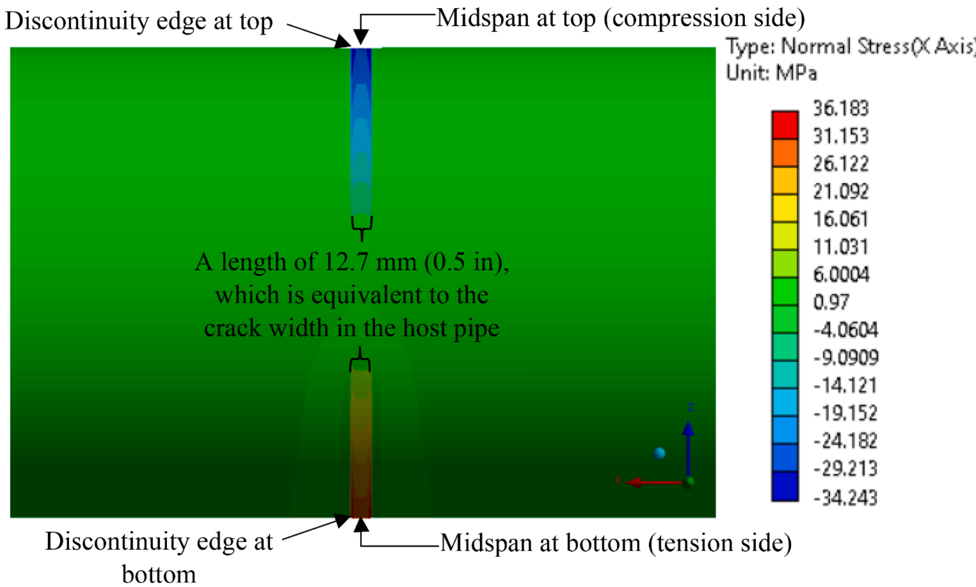

Fig. 17. Stress at the discontinuity edge and midspan at the top and bottom of IRP in host pipe with 0.5 in discontinuity width under bending (host pipe segments are temporarily hidden).

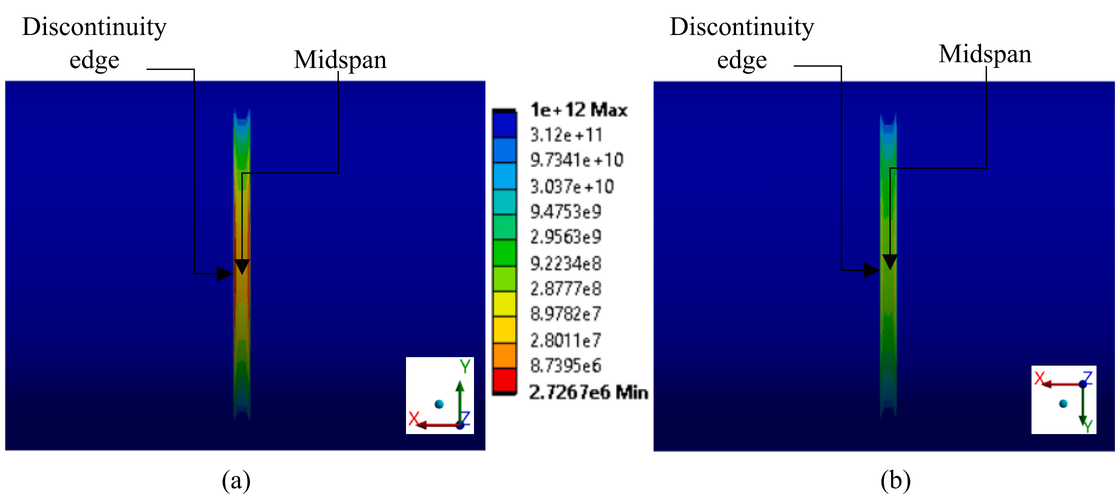

Fig. 18. Fatigue life contour plot (a) bottom (b) top of IRP at midspan (host pipe segments are temporarily hidden).

Table 6
Fatigue life at different locations of IRP.

Location	Fatigue life cycles
Discontinuity edge at the tension side of IRP	2.727e + 006
Discontinuity edge at the compression side of IRP	6.711e + 007
Midspan at the tension side of IRP	9.489e + 007
Midspan edge at the compression side of IRP	5.568e + 008

exceed the design life of one million cycles, according to the Fig. 23. To investigate the influence of other parameters, a discontinuity width of 12.7 mm (0.5 in) is employed since the minimum fatigue life of IRP is not significantly affected by the width of host pipe discontinuity.

Fig. 20 shows that increasing the discontinuity width from zero (continuous host pipe) to 12.7 mm (0.5 in) raises the stress at the midspan of IRP by 137 times. This indicates that stress concentration in IRP caused by a discontinuous host pipe segment leads to a substantial increase in the stress level at the midspan, particularly when the discontinuity width is narrower. However, stress at the midspan exhibits a nonlinear decrease as the discontinuity width increases from 12.7 mm (0.5 in) to 25.4 mm (1 in), followed by a linear reduction until the discontinuity width approaches 152.4 mm (6 in). Also, the midspan of the IRP experiences 41.1 % higher stress when the discontinuity width is 12.7 mm (0.5 in) compared to the system with a discontinuity width of 152.4 mm (6 in). Furthermore, as depicted in Fig. 24, unlike the system with a discontinuity width of 12.7 mm (0.5 in), in the system with a discontinuity width of 152.4 mm (6 in), the concentrated stress in IRP dissipates significantly over a length of 26.2 mm (1 in.) form the discontinuity edge before reaching a stable state that persists until midspan. The observed behaviour may be related to the fact that, as the width of circumferential discontinuity in the host pipe increases, the stress flow lines, which were densely packed together in IRP at the discontinuity edge, become more evenly distributed as they move away from the transition zone towards the midspan. This results in a greater reduction in localised stresses. On the other hand, when the discontinuity widths are relatively small, these widths may not be adequate for the densely packed stress flow lines to be uniformly distributed as they move towards the midspan. Consequently, the reduction in localised stress is diminished. Subsequently, if the discontinuity width reduces, there will be a substantial decline in the associated fatigue life at the

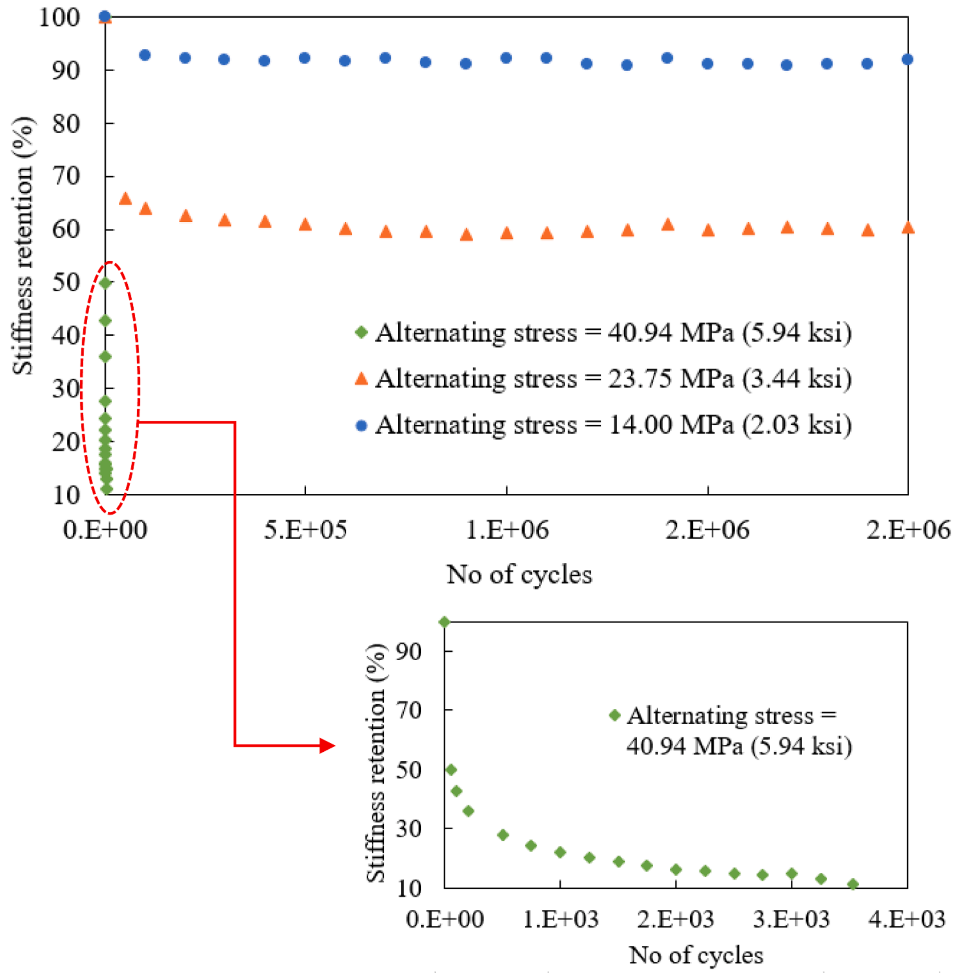

Fig. 19. Percentage stiffness retention of ALTRA10 coupons against the number of loading cycles at the three different applied alternating stress levels during the laboratory tension–tension fatigue tests.

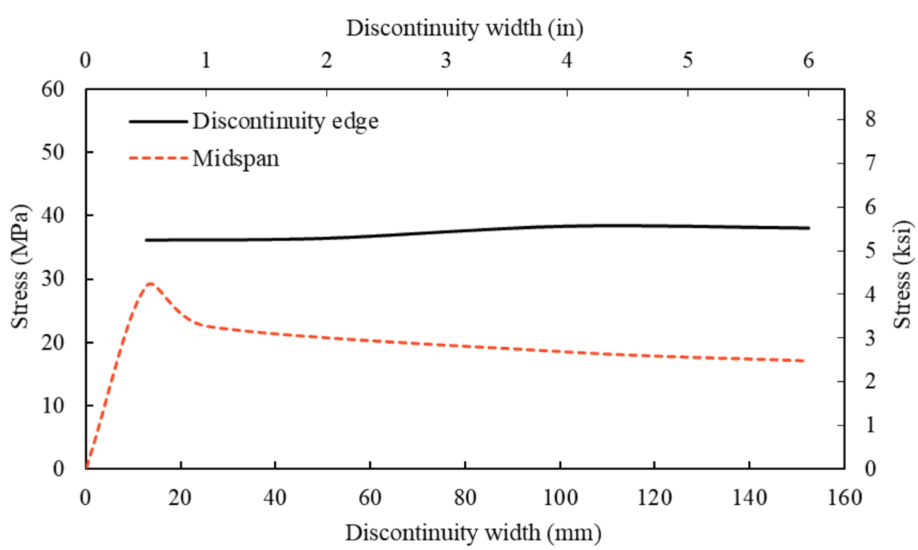

Fig. 20. Stress in IRP at the discontinuity edge and midspan at the bottom under a cyclic load of 14.8 kN (3.3 kips).

midspan (Fig. 23).

Fig. 25 shows the increase in stresses at the discontinuity edge and midspan of the compound IRP systems with varying discontinuity widths, relative to the maximum stress generated in IRP alone. Under the same load, the critical stresses in IRPs installed in discontinuous host pipe segments are around 120 times greater than the maximum stress developed in an IRP alone. The findings indicate that the service life of the IRP can be significantly reduced due to the presence of the host pipe

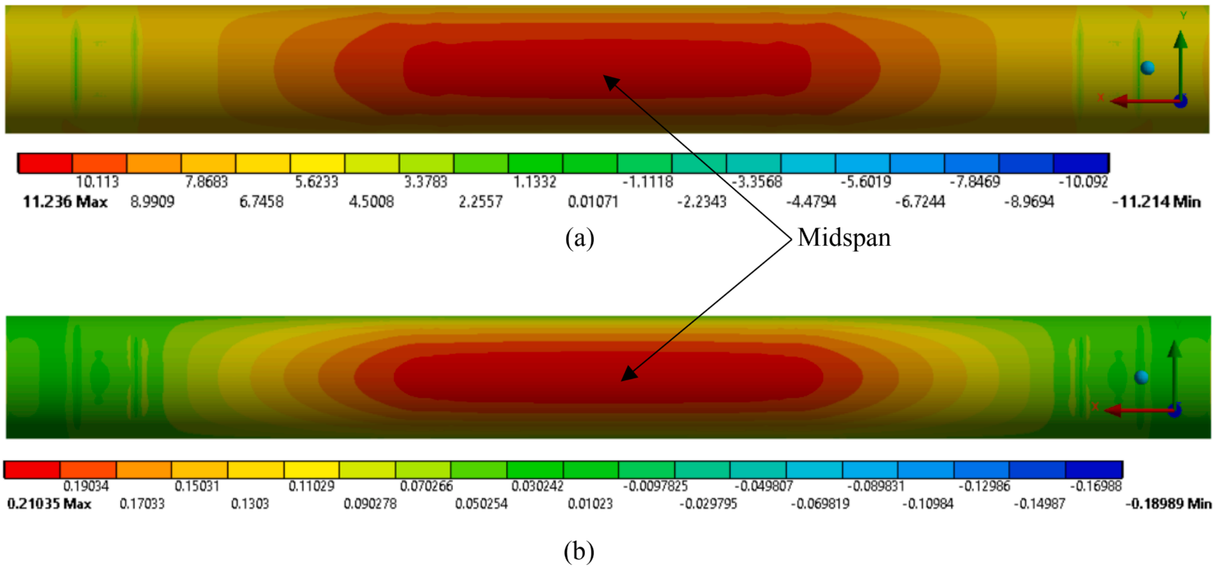

Fig. 21. Normal stress (x-axis) at the bottom of (a) continuous host pipe (b) IRP of the continuous host pipe repaired with IRP system under traffic loading [units: MPa].

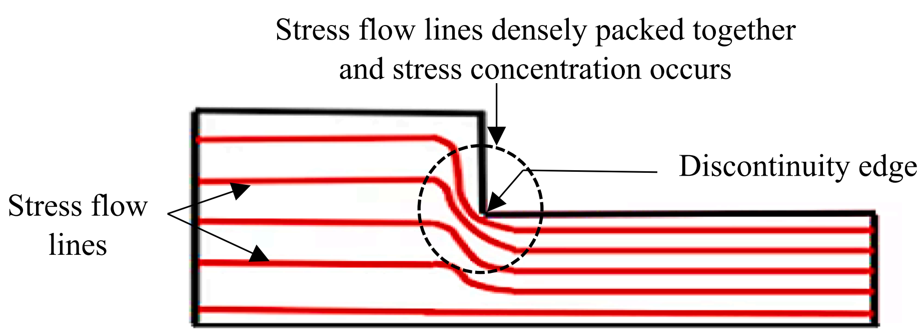

Fig. 22. Stress flow lines and stress concentration.

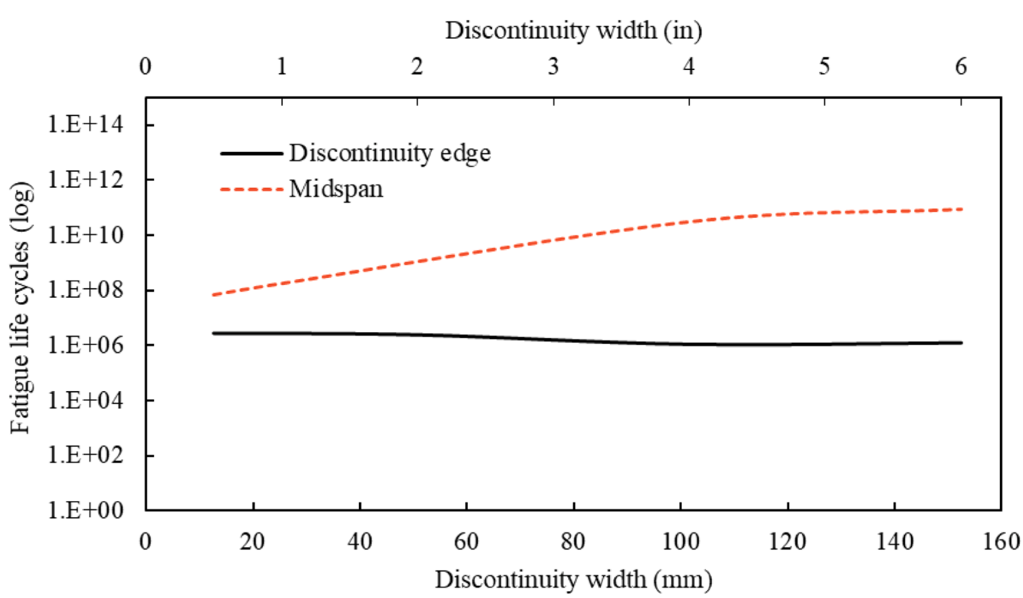

Fig. 23. Fatigue life at the discontinuity edge and midspan at the bottom under a cyclic load of 14.8 kN (3.3 kips).

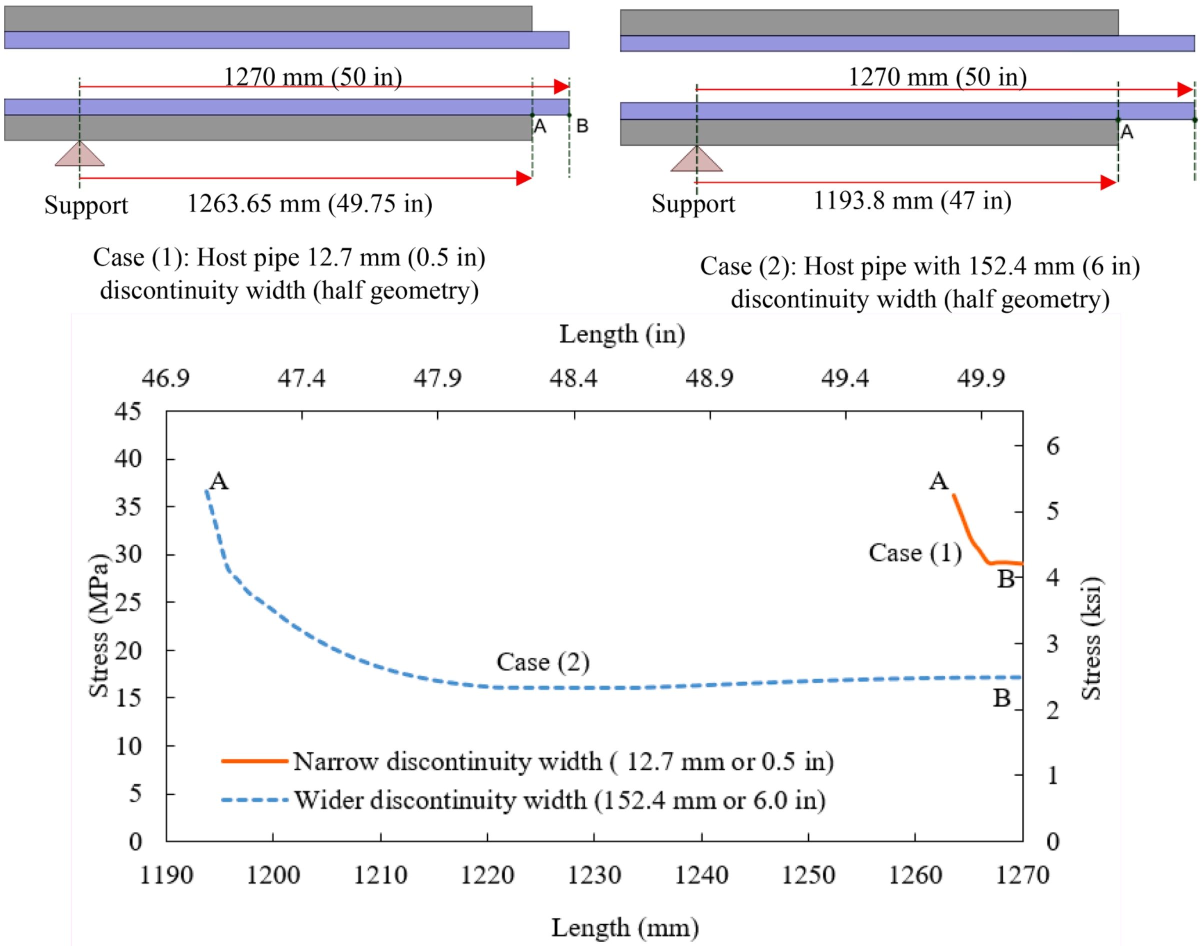

Fig. 24. Stress distribution at the bottom of IRP, from discontinuity edge to midspan for host pipe with narrow and wider discontinuity widths (length is measured from left support).

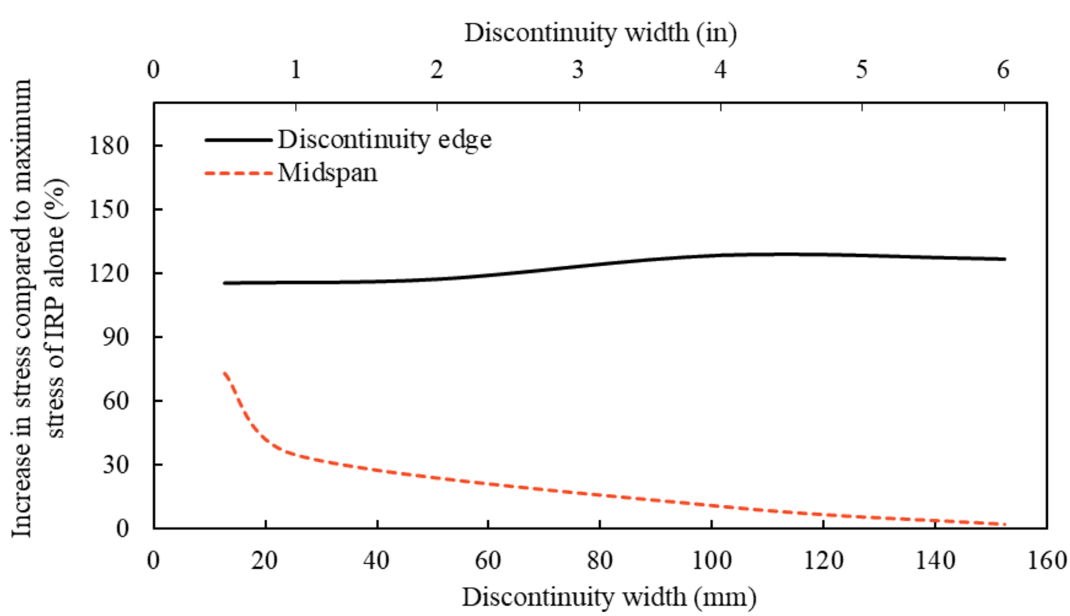

Fig. 25. Percentage increase in stress of IRP in damaged host pipe compared to the maximum stress generated in IRP alone under a cyclic load of 14.8 kN (3.3 kips).

with circumferential discontinuity, and this should be taken into consideration during the design and development of a repair system. It is also seen that the stresses generated at the midspan of IRP with the narrowest discontinuity width and widest discontinuity width under consideration are respectively 72.9 % and 1.8 % greater than that of IRP alone (Table 7). This result shows that, as the discontinuity width

Table 7
Percentage increase midspan stress of IRPs in discontinuous host pipes relative to the maximum stress in IRP alone, subjected to a traffic load of 14.8 kN (3.3 kips).

Width of host pipe discontinuity		% increase in midspan stress compared to maximum stress in IRP alone
mm	in	
12.7	0.5	72.9
25.4	1	34.6
50.8	2	21.5
101.6	4	10.3
152.4	6	1.8

widens the stress at the midspan approaches that of IRP alone. Compared to the IRP in continuous host pipe, the maximum stress produced in IRP alone is 78.8 times higher. However, unlike IRP in discontinuous host pipes, both IRP alone and IRP in continuous host pipes have significantly longer service lifespans exceeding one billion load cycles as they do not experience stress concentrations. In addition, Fig. 26 shows the level of maximum deformation for these systems. Accordingly, the lateral deformation at the discontinuity edge and midspan of the IRP system increases almost linearly with the widening of discontinuity. Even the maximum deformation level attributed to the system with a discontinuity width of 152.4 mm (6 in) is less than 4 mm (0.157 in), which is quite minimal.

3.2. Effect of IRP thickness and MOE

The effect of repair thickness on the maximum strain of IRP (at the edge of the circumferential discontinuity) made from different material systems is shown in Fig. 27. As can be seen, the maximum strain in IRP decreases nonlinearly as the repair thickness increases. This is because increasing the thickness of the IRP improves its stiffness, which reduces deformation. In addition, IRP systems generate their maximum strain when the repair thickness is minimal. Furthermore, it can also be seen from the graph that the maximum strain in the polymer system exceeds the design strain limit of 0.02 when the repair thickness is less than 4.115 mm (0.162 in) due to its low MOE, i.e. 1.744 GPa (253 ksi). Fig. 28 depicts how the tensile stress concentration at the discontinuity edge varies with increasing IRP thickness. The graph demonstrates that, for all repair materials, the stress concentration at the discontinuity edge diminishes nonlinearly and gradually as the repair thickness increases. IRP will experience high stress when the repair thickness is low. This is because, compared to damaged host pipes with thick IRP, the stress flow lines in those with thin IRP are more densely packed due to a greater reduction in total cross-sectional area at the discontinuity edge. As the repair thickness increases from 3.175 mm (0.125 in) to 9.525 mm (0.375 in), the total reduction in stress concentration in IRP systems with different repair materials varies between 46.6 % and 64.2 %. This variation is related to the fact that stress concentration appears to be influenced by the MOE of repair materials, as explained in subsequent sections.

Fig. 29 illustrates the relationship between the MOE and the strain of the IRP at the edge of the host pipe discontinuity (It is important to note that this figure is derived from an analysis conducted on IRP systems in steel host pipes). At the same thickness, polymeric IRP with the lowest MOE produces the highest strain at the discontinuity edge. When MOE increases from 1.744 GPa (253 ksi) to 7.9 GPa (1,146 ksi), the strain at the discontinuity edge decreases dramatically for all IRP thicknesses. From MOE of 26.43 GPa (2,035 ksi), a slight nonlinear reduction in strain is observed, followed by a linear decline until MOE of 200 GPa (29,008 ksi). This shows that IRP with low MOE deforms easily under low levels of load. A small increase in MOE substantially improves the resistance to deformation. IRP materials with higher elastic moduli, i.e greater than 26.43 GPa (2,035 ksi), on the other hand, are hard to deform under a traffic load of 14.8 kN (3.3 kips) and require a high load to experience significant strain. The overall reduction in the strain at the discontinuity edge as the MOE rises from 1.744 GPa (253 ksi) to 200 GPa (29,008 ksi) is the same for each IRP thickness, which is roughly 99 %. The influence of the MOE of IRP on the stress concentration for various repair thicknesses is shown in Fig. 30. According to that when the MOE rises, the stress concentration exhibits a slight nonlinear drop up to a MOE of 38.63 GPa (5,603 ksi) for repair thicknesses of 3.175 mm (0.125 in) and 4.115 mm (0.162 in) and up to a MOE of 26.43 GPa (2,035 ksi) for thicknesses of 6.35 mm (0.25 in) and 9.525 mm (0.375 in). From that point on, the stress concentration remains steady until the MOE of 200 GPa (29,008 ksi). The highest stress concentration at each repair thickness is observed in the polymeric IRP, which has the lowest MOE among all repair materials. This means that flexible IRP material can experience high stress concentration while stiff repair material can undergo lower stress concentration at the discontinuity edge. This is because stiff repair materials are more resistant to deformation than

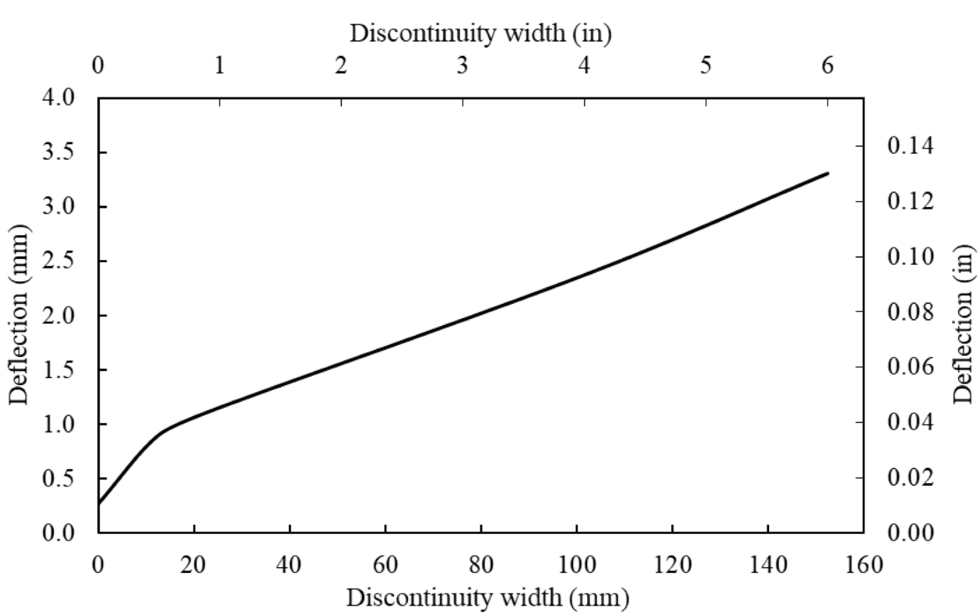

Fig. 26. Level of maximum deflection under a cyclic load of 14.8 kN (3.3 kips).

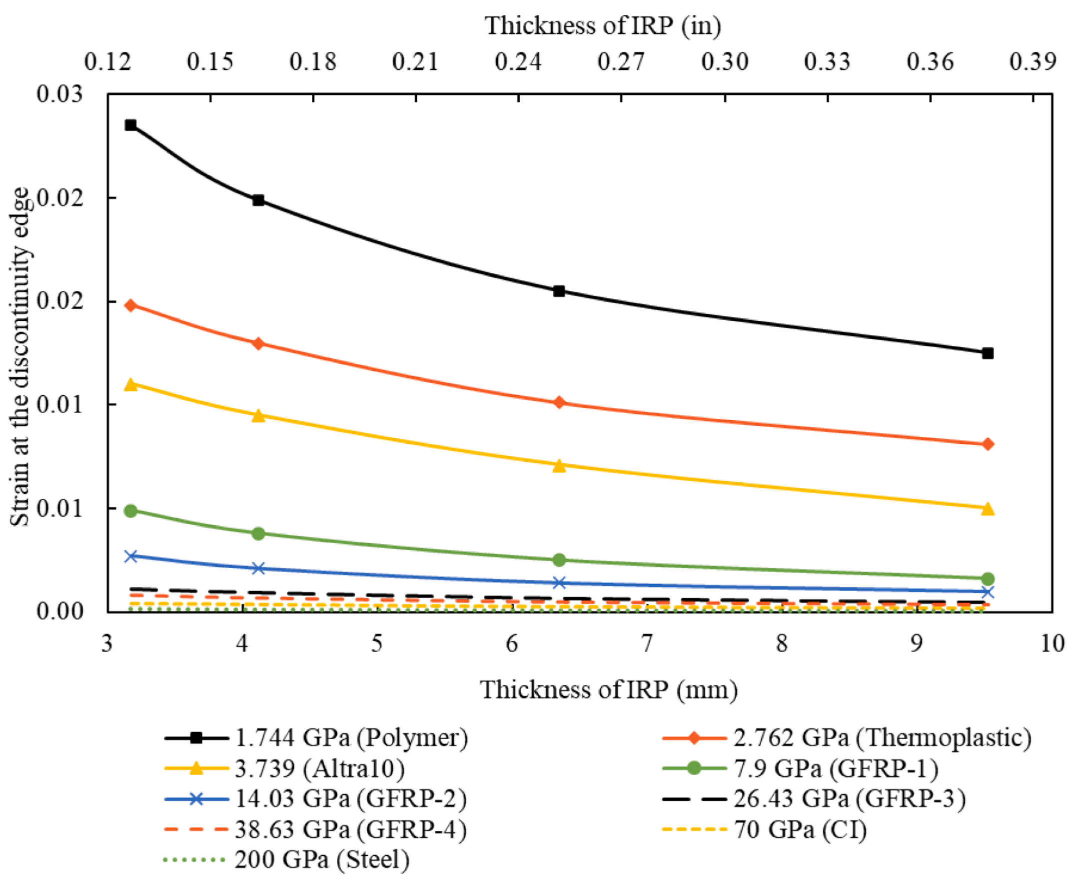

Fig. 27. Relationship of strain at the discontinuity edge and IRP thickness.

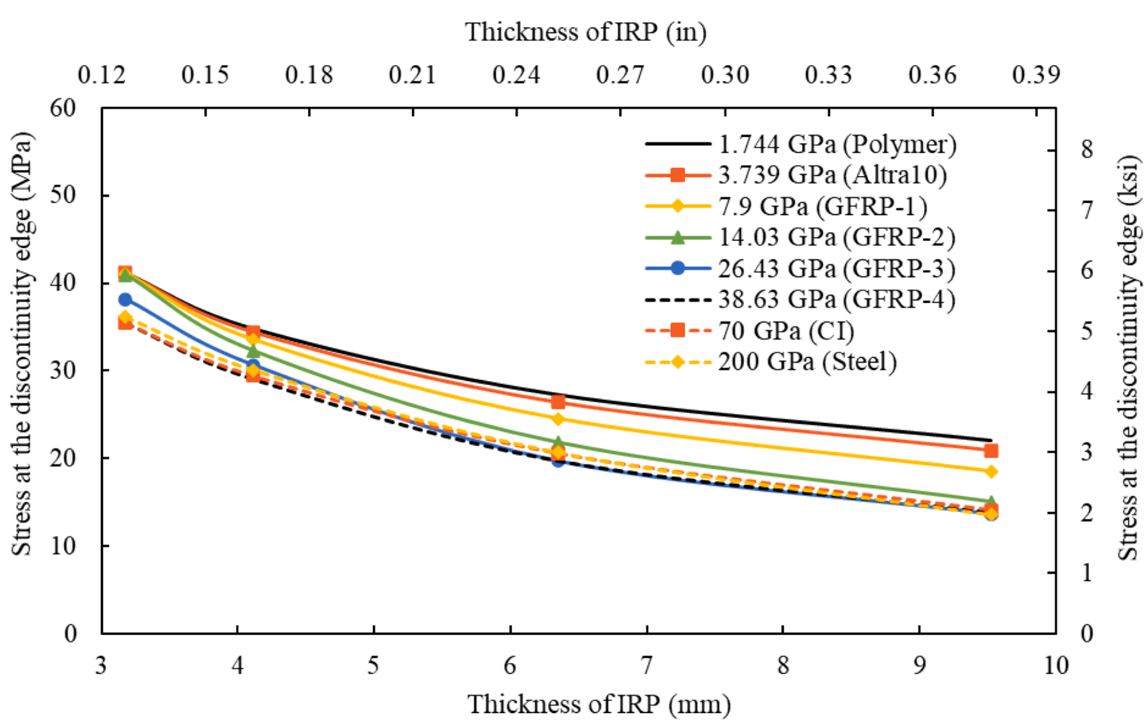

Fig. 28. Relationship of stress at the discontinuity edge and IRP thickness.

flexible repair materials, which undergo greater deformations or strain levels under the same applied load. As a consequence, in stiff IRP, stress is distributed more evenly at the discontinuity edge where the cross-sectional area changes, resulting in lower stress concentration than in flexible repair material systems.

Table 8 summarises the minimum loading cycles to failure of the IRP

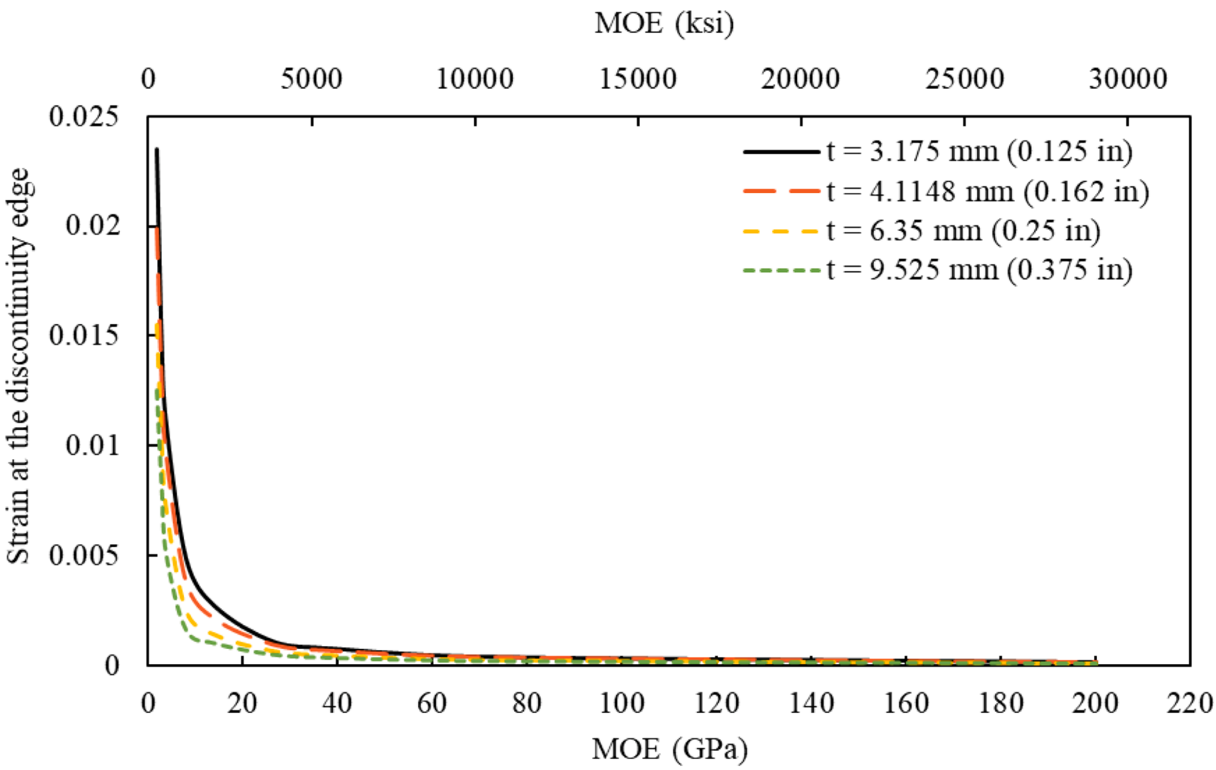

Fig. 29. Relationship of strain at the discontinuity edge and MOE of IRP.

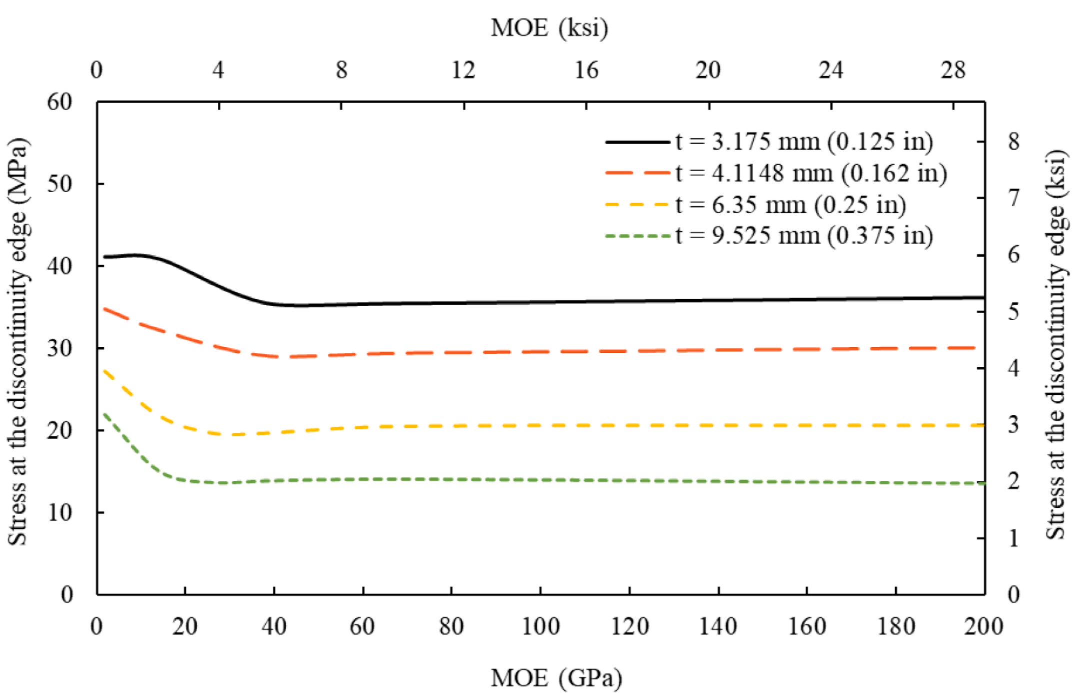

Fig. 30. Relationship of stress at the discontinuity edge and MOE of IRP.

systems installed in host pipes with circumferential discontinuities for various repair thicknesses and MOE based on the S-N curve of corresponding materials. The study found that the minimum fatigue life of IRP significantly extends with greater thickness and high MOE. This observation is in line with Huang et al [85], which concluded that the thickness of the composite pipe significantly increases its fatigue life, and with Tafsirojjaman et al [17], which demonstrated that an increase in both MOE and thickness of IRP leads to a significant improvement in fatigue life under cyclic bending. According to Table 8, among all the materials, the 3.175 mm (0.125 in) thick polymeric system has the lowest fatigue life which is only around 3 cycles during the traffic load under consideration. Based on the contour-plots in Fig. 31 (a), (b) and (c) respectively, in polymeric systems with 3.175 mm (0.125 in) and 4.115 mm (0.162 in) thickness, fatigue damage (at the bottom) would occur at the discontinuity edge and midspan during the service life, but only at the discontinuity edges with 6.35 mm (0.25 in) repair thickness.

Table 8
Minimum fatigue life of the IRP systems with different MOE and repair thicknesses.

Thickness of SIRP	Number of cycles 1.744 GPa (253 ksi) [Polymer]	3.739 GPa (542 ksi) [Altra10]	7.9 GPa (1,146 ksi) [GFRP-1]	14.03 GPa (2,035 ksi) [GFRP-2]	26.43 GPa (2,035 ksi) [GFRP-3]	38.63 GPa (5,603 ksi) [GFRP-4]	70 GPa (10,153 ksi) [CI]	200 GPa (29,008 ksi) [Steel]
3.175 mm (0.125 in)	3	2.684e + 005	>1E + 09	>1E + 09	>1E + 09	>1E + 09	>1E + 09	>1E + 09
4.115 mm (0.162 in)	130	2.727E + 06	>1E + 09	>1E + 09	>1E + 09	>1E + 09	>1E + 09	>1E + 09
6.35 mm (0.25 in)	26,209	7.165E + 07	>1E + 09	>1E + 09	>1E + 09	>1E + 09	>1E + 09	>1E + 09
9.525 mm (0.375 in)	2.048e + 006	1.519 + 09	>1E + 09	>1E + 09	>1E + 09	>1E + 09	>1E + 09	>1E + 09

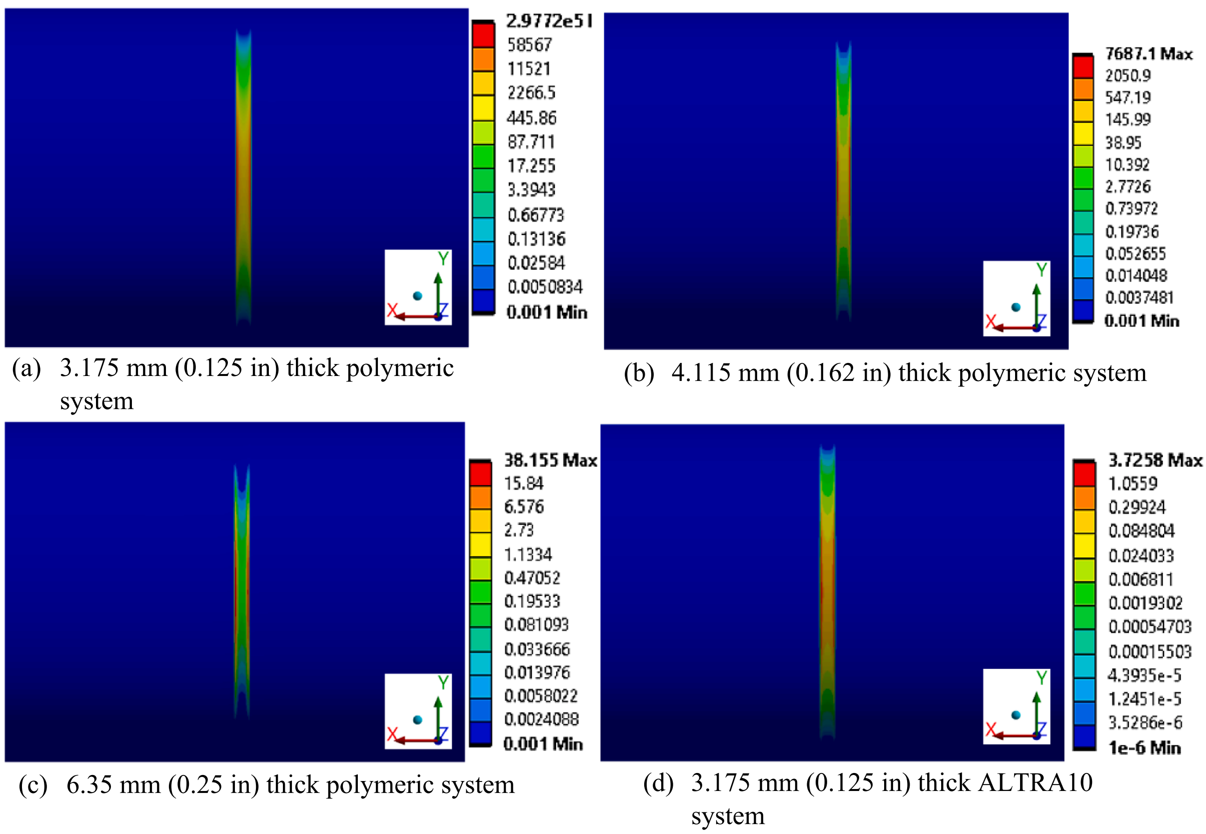

(a) 3.175 mm (0.125 in) thick polymeric system

(b) 4.115 mm (0.162 in) thick polymeric system

(c) 6.35 mm (0.25 in) thick polymeric system

(d) 3.175 mm (0.125 in) thick ALTRA10 system

Fig. 31. Fatigue damage of IRP at the bottom at midspan during the service life of 1 million loading cycles (host pipe segments are temporarily hidden).

Therefore, to achieve the targeted life of one million cycles, the polymeric IRP system with MOE of 1.744 GPa (253 ksi) requires a minimum repair thickness of 8.4 mm (0.331 in).

On the other hand, a 3.175 mm (0.125 in) thick ALTRA10 IRP system will fail after 268,400 fatigue cycles. The fatigue damage contour-plot for the bottom of the ALTRA10 IRP system in Fig. 31(d) shows that during the service life, only the discontinuity edge will experience fatigue damage (damage factor > 1.0) whereas there will be no damage to the midspan. Additionally, in order to use ALTRA10 as the repair material and achieve the intended fatigue life of one million cycles, the repair thickness must be at least 3.7 mm (0.146 in). Additionally, Fig. 32 displays the potential maximum stiffness degradation as a percentage, which IRP with a thickness of 4.115 mm (0.162 in) or greater might experience during its service life. This stiffness degradation is obtained through linear extrapolation of the data set from Fig. 19, based on the maximum alternating stresses obtained from FE simulations and service life of one million cycles. Accordingly, the stiffness degradation decreases nonlinearly and gradually as the repair thickness increases. The overall reduction in stiffness degradation when the IRP thickness increases from 4.115 mm (0.162 in) to 9.525 mm (0.375 in) is around 88 %. Moreover, the findings reveal that when the MOE of the IRP material increases, the thickness required to meet the targeted life reduces. Even with an IRP thickness of 3.175 mm (0.125 in), all other IRP material systems, those with a MOE of 7.9 GPa (1,146 ksi) or higher, will exceed the design fatigue life of one million cycles under the traffic load of 14.8 kN (3.3 kips).

3.3. Effect of loading level and critical loadings

The effect of loading level on the fatigue life of an IRP system with different repair thicknesses and MOE representing polymeric, ALTRA10, GFRP, and metallic is shown in Fig. 33 a, b, c and d, respectively. All IRP material systems regardless of their thickness indicate that a slight increase in lateral loading significantly shortens the fatigue life, and the responses are slightly nonlinear, even on semi-log plots. This finding is similar to that of Huang et al [85], who demonstrated that composite pipe had a considerably shorter fatigue life under cyclic bending as the imposed stress level increased. This decrease in fatigue life is caused by the significant rise in tensile stress concentration, which is directly related to the applied load. As a result, the minimum repair thickness that must be utilized for each repair material increases significantly. While increasing repair thickness prolongs the fatigue life, it can also be

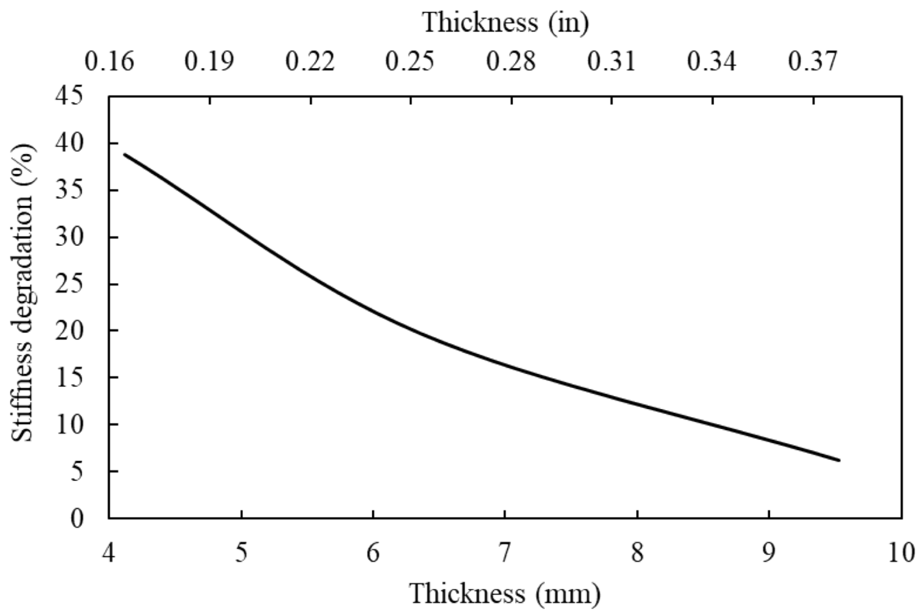

Fig. 32. Stiffness degradation of ALTRA10 IRP systems with different thicknesses at one million cycles.

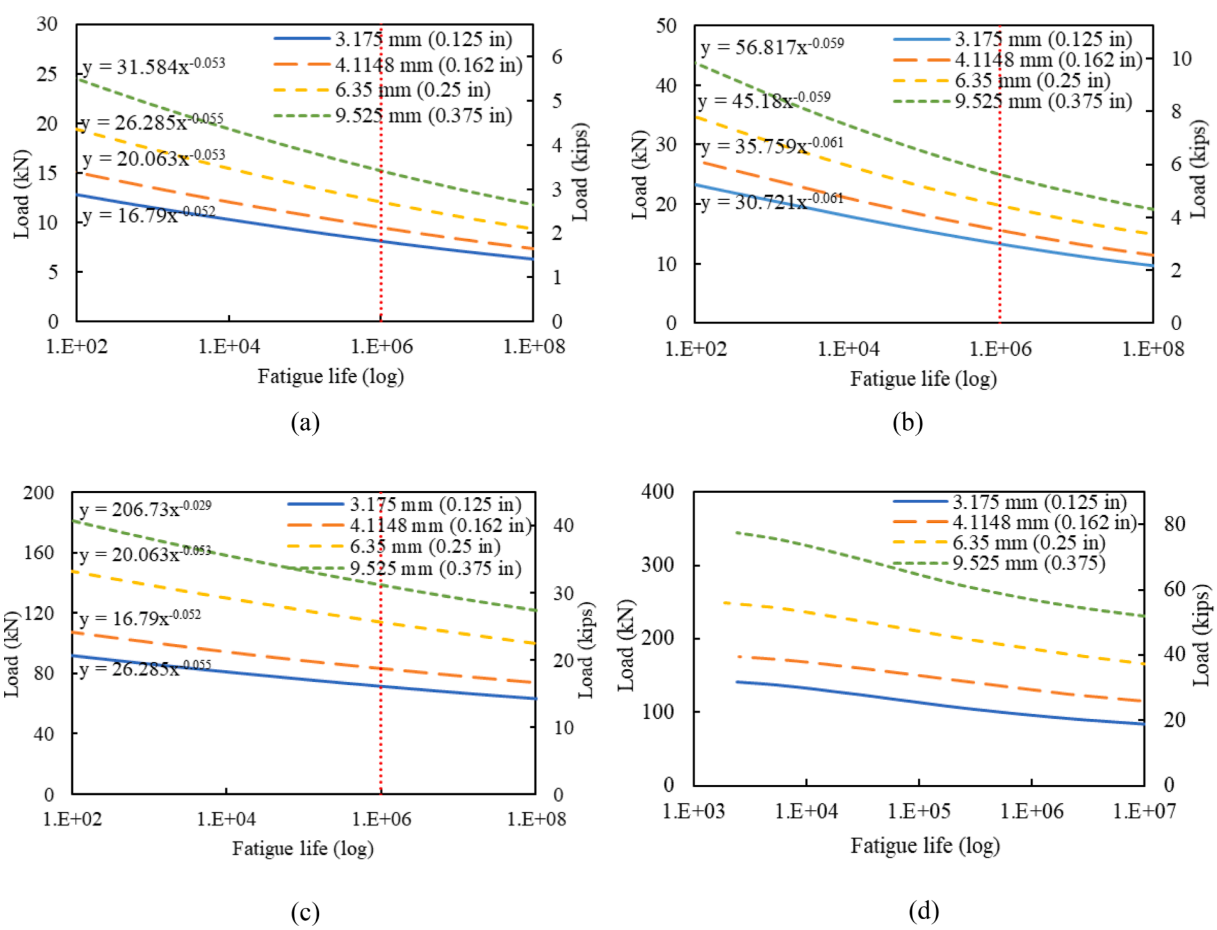

Fig. 33. Effect of loading level on the fatigue life of (a) polymeric (MOE of 1.744 GPa or 253 ksi), (b) ALTRA10 (MOE of 3.739 GPa or 542 ksi), (c) GFRP (MOE of 38.63 GPa or 5,603 ksi) (d) metallic (MOE of 200 GPa or 29,008 ksi) IRP repair systems.

problematic in practice due to potential reduction in flow capacity and increased cost. From these graphs, the maximum load that can be applied to various IRP systems to meet the desired design life of one million cycles are plotted against the MOE and thickness of the IRP, as shown in Fig. 34 and Fig. 35, respectively. According to Fig. 34, the critical load required to achieve the projected design of IRP systems dramatically increases when the MOE rises from 1.744 GPa (253 ksi) to 3.739 GPa (542 ksi) as a result of a substantial drop in the tensile stress

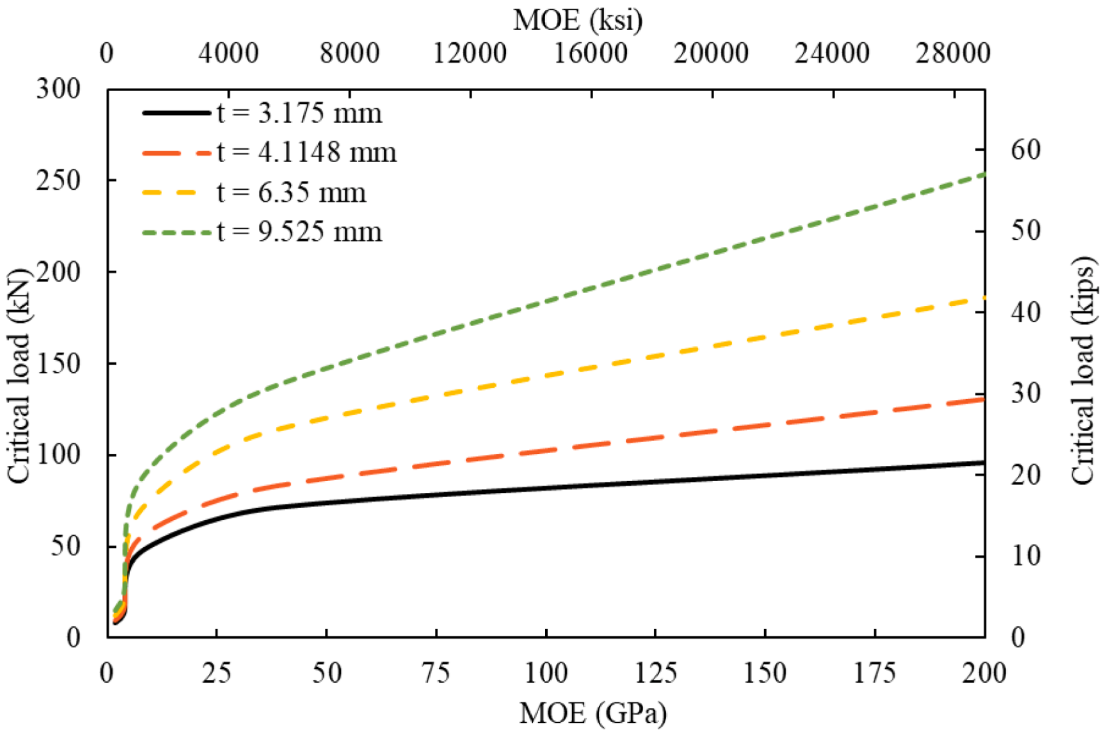

Fig. 34. Effect of the MOE on the critical lateral cyclic loading.

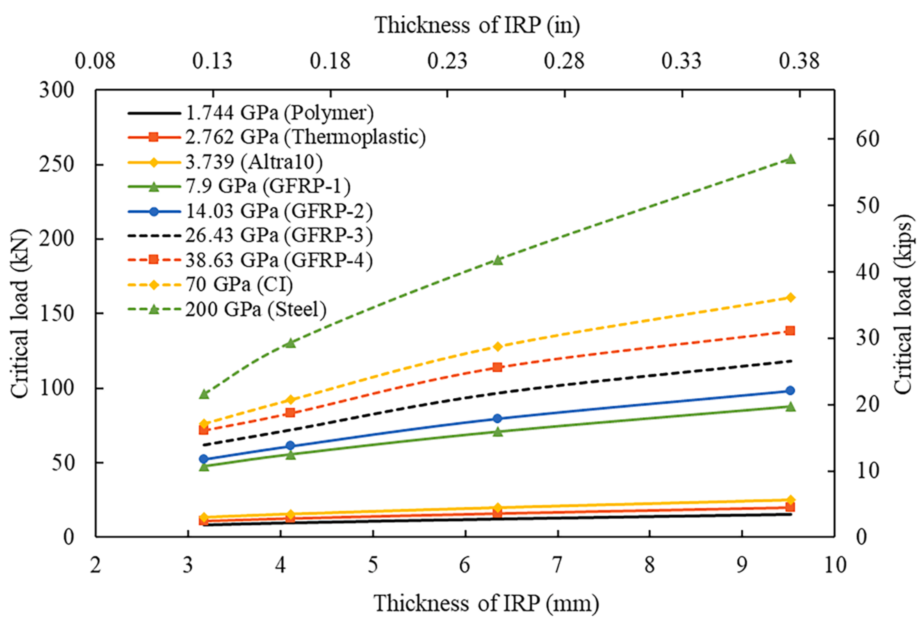

Fig. 35. Effect of the repair thickness on the critical lateral cyclic loading.

concentration, which controls the fatigue failure of IRP systems. Thereafter, it exhibits a nonlinear increase up to 38.63 GPa (5,603 ksi), followed by a linear increase up to 200 GPa (29,008 ksi). The maximum overall increment in critical load as the MOE increases from 1.744 GPa (253 ksi) to 200 GPa (29,008 ksi) is around 99 %. According to Fig. 35, the critical load displays a slightly nonlinear increase with increasing thickness, with an overall growth range between 84 % and 164 %. This is related to a reduction in the maximum stiffness degradation of IRP and the lowering in the density of the stress flow lines at the discontinuity edge as repair thickness increases.

3.4. *Quantifying the influence of investigated parameters*

Multiple regression analysis is carried out to quantify the influence of investigated parameters in this study using the SPSS (Statistical Package for the Social Sciences) statistical analysis software [86]. The investigated parameters are ranked based on their relative contribution to the fatigue strength of IRPs installed in host pipes with circumferential discontinuities during bending fatigue using the standardized coefficients or beta coefficients obtained from the multiple regression analysis, as suggested by Freedman [87]. Two regression analyses are performed, with the dependent variable being the maximum stress

Table 9
Summary[b] of models.

Model	R	R Square	Adjusted R Square	Std. Error of the Estimate
1	0.940[a]	0.883	0.881	11.096
2	0.935[a]	0.874	0.872	5.211

[a] Predictors: (constant), level of load (kN), MOE of IRP (GPa), thickness of IRP (mm).
[b] Dependent variable: maximum stress (MPa) or minimum fatigue life of IRP (cycles).

Table 10
ANOVA[a] of models.

Model		Sum of Squares	df	Mean Square	F	Sig.
1	Regression	144742.610	3	48247.537	391.851	<0.001[b]
	Residual	19207.831	156	123.127		
	Total	163950.441	159			
2	Regression	33167.352	3	11055.784	407.194	<0.001[b]
	Residual	4778.603	176	27.151		
	Total	37945.955	179			

[a] Dependent variable: maximum stress (MPa) or minimum fatigue life of IRP (cycles).
[b] Predictors: (constant), level of load (kN), MOE of IRP (GPa), thickness of IRP (mm).

(model 1) or the minimum fatigue life (model 2). In both regression models, repair thickness, MOE of the repair material, and level of loading are the independent variables. The reason for using two dependent variables is that changes in repair thickness, MOE of repair material, and loading affect maximum stress and minimal fatigue life differently. Therefore, the relative contribution of these parameters to maximum stress and fatigue life may differ. Since the study already revealed that changing the discontinuity width has almost no noticeable effect on the stress concentration and fatigue life under cyclic bending, it is recognised as the least important parameter and is eliminated from the regression analysis. Table 9 contains a summary of the multiple regression model 1 and 2. According to the statistical results, when taken as a group, the repair thickness, MOE of the repair material, and loading level in model 1 account for 88.3 % ($R^2 = 0.883$) of the variance in the maximum stress of IRP in the damaged host pipe, whereas those in model 2 account for 87.4 % ($R^2 = 0.874$) of the variance in the minimum fatigue life, which is good in practice. The results of the one-way ANOVA global test in Table 10 also indicate that, overall, the regression models 1 and 2 are statistically significant with F (3,156), $p < 0.001$, $R^2 = 0.883$ (tested using a significance level of 0.05) and F (3,176), $p < 0.001$, $R^2 = 0.874$, respectively. Therefore, when considered together, the repair thickness, the MOE of the repair material, and the loading level can predict the maximum stress and the minimum fatigue life of IRP in discontinuous host pipe significantly.

Table 11 shows the coefficient of the regression models. The significance levels reported in this table indicate that, when considered individually, the repair thickness, MOE of the repair material, and loading level all contribute to a significant amount of unique variance in maximum stress and minimum fatigue life of IRP in host pipe with circumferential discontinuity under lateral loading. Table 11 also displays the standardised beta coefficients, which compare the strength of the effect of the individual independent variable on the dependent variable. Accordingly, absolute standardised beta coefficients of the MOE of repair material, repair thickness and level of a load of regression model 1 are, respectively, 0.104, 0.425 and 0.851 while those of model 2 are, respectively, 0.897, 0.155 and 0.703. The findings demonstrate that the level of load, which has the highest standardized beta coefficient in model 1, is the parameter that contributes mostly to maximum stress. However, it is the second-most significant parameter that contributes to minimum fatigue life in model 2. This result can be explained by the fact that the imposed load level dominates the contribution to maximum stress, as it is related to the moment capacity of the cross-section of the system, which is a significant component of normal stress induced during bending. On the other hand, the MOE of the repair material, which has the lowest absolute standardised beta coefficient, is the parameter that has the least effect on the maximum stress generated in the IRP repair system. However, it is discovered to be the most important parameter in model 2, which has the greatest effect on the minimum fatigue life. This is because the maximum stress developed in IRP with the same thickness but different MOE in the elastic region only slightly varies under the same repetitive loading. In contrast, the corresponding fatigue life at the same alternating stress changes greatly when MOE changes. This is due to the fact that repair materials with higher MOE are better able to resist the deformation produced by the loading cycles and therefore have a reduced probability of failure in comparison to repair materials with lower MOE. As in model 1, the repair thickness is the parameter that has the second-largest influence on the maximum stress, but in model 2 it is the parameter that has the least impact on the minimum fatigue life. Due to its relationship to the moment of inertia of the repair cross-section, which is a component of bending stress, repair thickness has a relatively greater impact on maximum stress than it does on fatigue life. It is important to note however that using metallic materials such as cast iron and steel, which have the highest MOE among the repair materials considered, may not be the best choice. Water and gas pipelines are operating in harsh service environmental conditions (temperature, hygrothermal) which can accelerate the corrosion of steel and cast iron and can lead to premature fatigue failure.

4. Conclusion

Numerical simulations through finite element analyses were implemented to investigate the bending fatigue behaviour of a continuous host pipe with IRP, host pipes with circumferential discontinuities repaired with IRPs, and IRP alone (without host pipe). The influence of the discontinuity width of the host pipe, thickness and elastic modulus of the repair material, and level of imposed loading, were thoroughly examined. Multiple regression statistical analysis was utilised to determine which of the investigated parameters has a significant effect on

Table 11
Coefficients[a] of models.

Model		Unstandardized Coefficients B	Unstandardized Coefficients Std. Error	Standardized Coefficients Beta	t	Sig.	Rank
1	(Constant)	31.684	2.770		11.440	<0.001	
	Level of load (kN)	1.994	0.065	0.851	30.517	<0.001	1
	MOE of IRP (GPa)	−0.051	0.014	−0.104	−3.721	<0.001	3
	Thickness of IRP (mm)	−5.561	0.359	−0.425	−15.497	<0.001	2
2	(Constant)	9.897	1.277		7.753	<0.001	
	Level of load (kN)	−0.743	0.030	−0.703	−24.720	<0.001	2
	MOE of PIP (GPa)	0.982	0.031	0.897	31.506	<0.001	1
	Thickness of IRP (mm)	0.906	0.157	0.155	5.771	<0.001	3

[a] Dependent variable: maximum stress (MPa) or minimum fatigue life of IRP (cycles).

stress concentration and fatigue life. Based on the findings of this investigation, the following conclusion can be drawn:

- Host pipe segments with circumferential discontinuities repaired with fully bonded IRP systems can be critical in bending fatigue due to the high stress concentration induced in IRP at the discontinuity edge. The stress concentration results in a reduction in the minimum fatigue life or failure before reaching the desired design life. It is essential therefore to minimise stress concentration when designing an IRP system to be installed in host pipe segments with circumferential discontinuity to avoid premature fatigue failure under cyclic bending.
- The continuity of the host pipe stabilises the stress generated in the IRP during bending, thereby extending fatigue life and reducing fatigue failure.
- The stress and the fatigue life at the midspan of the repair system become closer to that of IRP alone for wide discontinuity widths.
- The width of the circumferential discontinuity in the host pipe has no significant effect on the level of stress concentration in IRP at the discontinuity edge indicating that the fatigue failure of fully bonded IRP systems with varying discontinuity widths may occur at around the same service life.
- The minimum fatigue life of IRP systems with discontinuous host pipes significantly extends as the thickness and MOE of repair material increase, under the same loading due to the reduction in stress concentration at the discontinuity edge at the bottom. The polymeric IRP system with a MOE of 1.744 GPa (253 ksi) requires a minimum repair thickness of 8.4 mm (0.331 in), whereas an ALTRA10 IRP with a MOE of 3.739 GPa (542 ksi) requires a repair thickness of at least 3.7 mm (0.146 in) under a repetitive traffic load of 14.8 kN (3.3 kips) to reach the intended life of one million cycles.
- Under the traffic load of 14.8 kN (3.3 kips), the ALTRA10 IRP material system with a thickness of 4.115 mm (0.162 in) will experience a 38 % reduction in stiffness at one million fatigue cycles. This stiffness reduction is heavily influenced by the stress concentration in the IRP at the edge of circumferential host-pipe discontinuity. Increasing the IRP thickness to 9.525 mm (0.375 in) reduced the stiffness loss by 88.0 %.
- The level of loading has a significant effect on fatigue life. A high level of applied load shortens the fatigue life of IRP regardless of repair thickness or MOE of repair material.
- Multiple regression analysis indicated that the maximum stress generated in IRP systems during bending fatigue is significantly affected by the level of load, followed by repair thickness, MOE, and discontinuity width. On the other hand, the MOE of the IRP is identified to have the greatest contribution to fatigue life, followed by the level of load, repair thickness, and discontinuity width.

The results of this study demonstrated that the material and geometrical properties of the IRP and the host pipe can influence the bending fatigue behaviour of the repaired system. Investigating the effects of other important design parameters such as Poisson's ratio of IRP materials and type of host pipes will provide a more detailed understanding of the bending fatigue behaviour of IRP-repaired discontinuous legacy pipe systems.

CRediT authorship contribution statement

Shanika Kiriella: Data curation, Investigation, Methodology, Software, Validation, Visualization, Writing – original draft, Writing – review & editing, Conceptualization. **Allan Manalo:** Conceptualization, Funding acquisition, Investigation, Methodology, Project administration, Supervision, Writing – original draft, Writing – review & editing. **Cam Minh Tri Tien:** . **Hamid Ahmadi:** Conceptualization, Investigation, Writing – review & editing, Methodology, Software, Supervision. **Patrick G. Dixon:** Conceptualization, Data curation, Investigation, Methodology, Writing – review & editing. **Warna Karunasena:** Conceptualization, Investigation, Methodology, Supervision, Writing – review & editing. **Ahmad Salah:** Conceptualization, Investigation, Methodology, Software. **Brad P. Wham:** Conceptualization, Funding acquisition, Methodology, Project administration, Resources, Writing – review & editing.

Declaration of competing interest

The authors declare that they have no known competing financial interests or personal relationships that could have appeared to influence the work reported in this paper.

Data availability

Data will be made available on request.

Acknowledgement

The information, data, or work presented herein was funded in part by the Advanced Research Projects Agency-Energy (ARPA-E), US Department of Energy, under Award Number DE-AR0001327 and Sanexen Environmental Services Inc. (Quebec, Canada). The views and opinions of authors expressed herein do not necessarily state or reflect those of the United States Government or any agency thereof.

References

[1] Dumitrescu A, Minescu M, Dinita A, Lambrescu I. Corrosion Repair of Pipelines Using Modern Composite Materials Systems: A Numerical Performance Evaluation. Energies 2021;14(3):615.

[2] Li X, Han Z, Zhang R, Abbassi R, Chang D. An integrated methodology to manage risk factors of aging urban oil and gas pipelines. J Loss Prev Process Ind 2020;66:104154.

[3] Duell JM, Wilson JM, Kessler MR. Analysis of a carbon composite overwrap pipeline repair system. Int J Press Vessel Pip 2008;85(11):782–8.

[4] Sinha SK, Pandey MD. Probabilistic Neural Network for Reliability Assessment of Oil and Gas Pipelines. Comput Aided Civ Inf Eng 2002;17(5):320–9.

[5] Mahmoodian M, Li C-Q. Structural integrity of corrosion-affected cast iron water pipes using a reliability-based stochastic analysis method. Struct Infrastruct Eng 2016;12(10):1356–63.

[6] Zhao W, Zhang T, Wang Y, Qiao J, Wang Z. Corrosion Failure Mechanism of Associated Gas Transmission Pipeline. Materials 2018;11(10):1935.

[7] Gamboa E, Linton V, Law M. Fatigue of stress corrosion cracks in X65 pipeline steels. Int J Fatigue 2008;30(5):850–60.

[8] Fang J, Cheng X, Gai H, Lin S, Lou H. Development of machine learning algorithms for predicting internal corrosion of crude oil and natural gas pipelines. Comput Chem Eng 2023;177:108358.

[9] Hussein Khalaf A, Xiao Y, Xu N, Wu B, Li H, Lin B, et al. Emerging AI technologies for corrosion monitoring in oil and gas industry: A comprehensive review. Eng Fail Anal 2024;155:107735.

[10] Akhi AH, Dhar AS. Fracture parameters for buried cast iron pipes subjected to internal surface corrosions and cracks. Journal of Pipeline Science and Engineering 2021;1(2):187–97.

[11] Mahmoodian M, Li C-Q. Failure assessment and safe life prediction of corroded oil and gas pipelines. J Pet Sci Eng 2017;151:434–8.

[12] Rajeev, P., J. Kodikara, D. Robert, P. Zeman, and B. Rajani. *Factors contributing to large diameter water pipe failure as evident from failure inspection.* 2013.

[13] Biezma MV, Andrés MA, Agudo D, Briz E. Most fatal oil & gas pipeline accidents through history: A lessons learned approach. Eng Fail Anal 2020;110:104446.

[14] Abd-Elhady AA, Sallam H-E-D-M, Alarifi IM, Malik RA, EL-Bagory TMAA. Investigation of fatigue crack propagation in steel pipeline repaired by glass fiber reinforced polymer. Compos Struct 2020;242:112189.

[15] Li B, Wang F, Fang H, Yang K, Zhang X, Ji Y. Experimental and numerical study on polymer grouting pretreatment technology in void and corroded concrete pipes. Tunn Undergr Space Technol 2021;113:103842.

[16] Shaukat MM, Ashraf F, Asif M, Pashah S, Makawi M. Environmental Impact Analysis of Oil and Gas Pipe Repair Techniques Using Life Cycle Assessment (LCA). Sustainability 2022;14(15):9499.

[17] Tafsirojjaman T, Manalo A, Tien CMT, Wham BP, Salah A, Kiriella S, et al. Analysis of failure modes in pipe-in-pipe repair systems for water and gas pipelines. Eng Fail Anal 2022;140:106510.

[18] Tien CMT, Manalo A, Dixon P, Tafsirojjaman T, Karunasena W, Flood WW, et al. Effects of the legacy pipe ends on the behaviour of pipe-in-pipe repair systems under internal pressure. Eng Fail Anal 2023;144:106957.

[19] Stewart, H.E., A.N. Netravali, and T.D. O'Rourke, *Performance Testing of Field-Aged Cured-in-Place Liners (CIPL) for Cast Iron Piping* 2015: School of Civil and Environmental Engineering, Cornell University p. 1-128.

[20] Dixon PG, Tafsirojjaman T, Klingaman J, Hubler MH, Dashti S, O'rourke TD, et al. State-of-the-Art Review of Performance Objectives for Legacy Gas Pipelines with Pipe-in-Pipe Rehabilitation Technologies. J Pipeline Syst Eng Pract 2023;14(2).

[21] Klingaman, J., P.G. Dixon, B.P. Wham, S. Dashti, and M.H. Hubler. *Traffic Loading Effects on Rehabilitated Cast Iron Distribution Pipelines*. in *Pipelines 2022*. 2022. Indianapolis, Indiana.

[22] Jeon S-S, O'Rourke TD, Neravali AN. Repetitive loading effects on cast iron pipelines with cast-in-place pipe lining system. J Transp Eng 2004;130(6): 692–705.

[23] Ha SK, Lee HK, Kang IS. Structural behavior and performance of water pipes rehabilitated with a fast-setting polyurea–urethane lining. Tunn Undergr Space Technol 2016;52:192–201.

[24] Ellison, D., F. Sever, P. Oram, W. Lovins, and A. Romer, *Global review of spray-on structural lining technologies*. 2010, EnvironmentalProtection Agency (USEPA) p. 1–158.

[25] Barros SD, Fadhil BM, Alila F, Diop J, Reis JML, Casari P, et al. Using blister test to predict the failure pressure in bonded composite repaired pipes. Compos Struct 2019;211:125–33.

[26] Beyene AT, Belingardi G. Bending fatigue failure mechanisms of twill fabric E-Glass/Epoxy composite. Compos Struct 2015;122:250–9.

[27] Lee H-G, Kang MG, Park J. Fatigue failure of a composite wind turbine blade at its root end. Compos Struct 2015;133:878–85.

[28] Muc A, Barski M, ChwbB M, Romanowicz PJ, Stawiarski A. Fatigue damage growth monitoring for composite structures with holes. Compos Struct 2018;189:117–26.

[29] Rafiee R. Stochastic fatigue analysis of glass fiber reinforced polymer pipes. Compos Struct 2017;167:96–102.

[30] Olamide A, Bennecer A, Kaczmarczyk S. Finite Element Analysis of Fatigue in Offshore Pipelines with Internal and External Circumferential Cracks. Applied Mechanics 2020;1(4):193–223.

[31] Song S, Zang H, Duan N, Jiang J. Experimental Research and Analysis on Fatigue Life of Carbon Fiber Reinforced Polymer (CFRP) Tendons. Materials 2019;12(20): 3383.

[32] Bennani, M., A.E. Akkad, and A. Elkhalfi, *Impact of an internal polymeric liner on the fatigue strength of pressure vessels under internal pressure*. 2016, WSEAS Transactions on Applied and Theoretical Mechanics. p. 1-9.

[33] O'Rourke TD, Netravali AN, Pendharkar SM, Toprak S, Tonkinson A, Chaudhuri D. Evaluating Service Life of Anaerobic Joint Sealant Products and Techniques. Chicago: Gas Research Institute; 1996.

[34] Brunbauer J, Stadler H, Pinter G. Mechanical properties, fatigue damage and microstructure of carbon/epoxy laminates depending on fibre volume content. Int J Fatigue 2015;70:85–92.

[35] Ansari MTA, Singh KK, Azam MS. Fatigue damage analysis of fiber-reinforced polymer composites—A review. J Reinf Plast Compos 2018;37(9):636–54.

[36] Ferdous W, Manalo A, Peauril J, Salih C, Raghava Reddy K, Yu P, et al. *Testing and modelling the fatigue behaviour of GFRP composites@ Effect of stress level, stress concentration and frequency*. Engineering Science and Technology, an. Int J 2020;23 (5):1223–32.

[37] Lai J, Huang H, Buising W. Effects of microstructure and surface roughness on the fatigue strength of high-strength steels. Procedia Struct Integrity 2016;2:1213–20.

[38] Brnic J, Turkalj G, Canadija M, Lanc D, Krscanski S, Brcic M, et al. Mechanical Properties, Short Time Creep, and Fatigue of an Austenitic Steel. Materials 2016;9 (4):298.

[39] Abdelhaleem AM, Megahed M, Saber D. Fatigue behavior of pure polypropylene and recycled polypropylene reinforced with short glass fiber. J Compos Mater 2018;52(12):1633–40.

[40] Chandran KSR. Mechanical fatigue of polymers: A new approach to characterize the SN behavior on the basis of macroscopic crack growth mechanism. Polymer 2016;91:222–38.

[41] Maiti S, Geubelle PH. A cohesive model for fatigue failure of polymers. Eng Fract Mech 2005;72(5):691–708.

[42] Sauer JA, Chen CC. Deformation modes and fatigue behavior in styrene-acrylonitrile and acrylonitrile-butadiene-styrene copolymers. Polym Eng Sci 1984; 24(10):786–97.

[43] Brostow W, Lobland HEH, Khoja S. Brittleness and toughness of polymers and other materials. Mater Lett 2015;159:478–80.

[44] Mellott, S.R., *Tensile, Creep, and Fatigue Behaviors of Thermoplastics Including Thickness, Mold Flow Direction, Mean Stress, Temperature, and Loading Rate Effects*, in *Graduate Faculty*. 2012, The University of Toledo. p. 328.

[45] Guo R, Li C, Niu YB, Xian G. The fatigue performances of carbon fiber reinforced polymer composites – A review. J Mater Res Technol 2022;21:4773–89.

[46] Lian W, Yao W. Fatigue life prediction of composite laminates by FEA simulation method. Int J Fatigue 2010;32(1):123–33.

[47] Colombi P, Fava G. Fatigue behaviour of tensile steel/CFRP joints. Compos Struct 2012;94(8):2407–17.

[48] Yin G-Q, Kang X, Zhao G-P. Fatigue Properties of the Ultra-High Strength Steel TM210A. Materials 2017;10(9):1057.

[49] Jiang R, Rathnayaka S, Shannon B, Zhao XL, Ji J, Kodikara J. Analysis of failure initiation in corroded cast iron pipes under cyclic loading due to formation of through-wall cracks. Eng Fail Anal 2019;103:238–48.

[50] Kiriella S, Manalo A, Tien CMT, Ahmadi H, Wham BP, Salah A, et al. Lateral deformation behaviour of structural internal replacement pipe repair systems. Compos Struct 2023;319:117144.

[51] Shou KJ, Chen BC. Numerical analysis of the mechanical behaviors of pressurized underground pipelines rehabilitated by cured-in-place-pipe method. Tunn Undergr Space Technol 2018;71:544–54.

[52] Yang K, Xue B, Fang H, Du X, Li B, Chen J. Mechanical sensitivity analysis of pipe-liner composite structure under multi-field coupling. Structures 2021;29:484–93.

[53] Yang K, Fang H, Bu J, Zhang X, Li B, Du X, et al. Full-scale experimental investigation of the mechanical characteristics of corroded buried concrete pipes after cured-in-place-pipe rehabilitation. Tunn Undergr Space Technol 2021;117: 104153.

[54] Brown MJP, Moore ID, Fam A. Performance of a cured-in-place pressure pipe liner passing through a pipe section without structural integrity. Tunn Undergr Space Technol 2014;42:87–95.

[55] Ansys, Finite Element Analysis (FEA) Software for Structuaral Engineering. 2021, ANSYS, Inc.

[56] Zhong Z, Wang S, Zhao Mi, Du X, Li L. Performance of ductile iron push-on joints rehabilitated with CIPP liner under repetitive and seismic loadings. Soil Dyn Earthq Eng 2018;115:776–86.

[57] Argyrou C, Bouziou D, O'Rourke TD, Stewart HE. Retrofitting pipelines with cured-in-place linings for earthquake-induced ground deformations. Soil Dyn Earthq Eng 2018;115:156–68.

[58] Zhong Z, Bouziou D, Wham B, Filiatrault A, Aref A, O'Rourke TD, et al. Seismic Testing of Critical Lifelines Rehabilitated with Cured in Place Pipeline Lining Technology. J Earthq Eng 2014;18(6):964–85.

[59] Shirazi H, Eadie R, Chen W. A REVIEW ON CURRENT UNDERSTANDING OF PIPELINE CIRCUMFERENTIAL STRESS CORROSION CRACKING IN NEAR-NEUTRAL PH ENVIRONMENT. Eng Fail Anal 2023;148:107215.

[60] Petersen, D.L., C.R. Nelson, G. Li, T.J. McGrath, and Y. Kitane, *Recommended Design Specifications for Live Load Distribution to Buried Structures*. 210, National Research Cooperative Highway Program: Washington, D.C.

[61] Gowtham KL, Srivatsa SR. Study of Convergence of Results in Finite Element Analysis of a Plane Stress Bracket. Journal of Engineering Research and Application 2018:7–12.

[62] Mellott SR, Fatemi A. Fatigue behavior and modeling of thermoplastics including temperature and mean stress effects. Polym Eng Sci 2014;54(3):725–38.

[63] Zakaria KA, Jimit RH, Ramli SNR, Aziz AA, Bapokutty O, Ali MB. Study On Fatigue Life And Fracture Behaviour Of Fibreglass Reinforced Composites. Journal of Mechanical Engineering and Sciences 2016;10(3):2300–10.

[64] Huh Y-H, Lee J-H, Kim D-J, Lee Y-S. Effect of stress ratio on fatigue life of GFRP composites for WT blade. J Mech Sci Technol 2012;26(7):2117–20.

[65] Seica MV, Packer JA. Mechanical Properties and Strength of Aged Cast Iron Water Pipes. J Mater Civ Eng 2004;16(1):69–77.

[66] Preedawiphat P, Mahayotsanun N, Sa-ngoen K, Noipitak M, Tuengsook P, Sucharitpwatskul S, et al. Mechanical Investigations of ASTM A36 Welded Steels with Stainless Steel Cladding. Coatings 2020;10(9):844.

[67] O'Rourke TD, Strait JE, Mottl N, Berger B, Wham B, Stewart HE, et al. Cornell University. NY: Ithaca; 2021.

[68] Matthews, J., W. Condit, R. Wensink, and G. Lewis, *Performance Evaluation of Innovative Water Main Rehabilitation Cured-in-Place Pipe Lining Product in Cleveland*. 2012, U.S. Environmental Protection Agency (EPA).

[69] Babu S, Hosamath M, Gai R. Fatigue Life Calculator for Ansys Workbench using ACT/PYTHON. International Journal of Engineering Research & Technology (IJERT) 2021;10(2):435–7.

[70] Murakami Y, Takagi T, Wada K, Matsunaga H. Essential structure of S-N curve: Prediction of fatigue life and fatigue limit of defective materials and nature of scatter. Int J Fatigue 2021;146:106138.

[71] Fajri A, Prabowo AR, Surojo E, Imaduddin F, Sohn JM, Adiputra R. Validation and Verification of Fatigue Assessment using FE Analysis: A Study Case on the Notched Cantilever Beam. Procedia Struct Integrity 2021;33:11–8.

[72] Hou Y, Lin HT. Fatigue Life Prediction Based on AMPS Stress-Life Approach Fatigue FEA. in *The 8th International Conference on Computational Methods (ICCM2017)*. 2017.

[73] ASTM, *ASTM D3479/D3479M-19*, in *Standard Test Method for Tension-Tension Fatigue of Polymer Matrix Composite Materials*. 2019, ASTM International. p. 1-6.

[74] Rausch T, Beiss P, Broeckmann C, Lindlohr S, Weber R. Application of quantitave image analysis of graphite structures for the fatigue strength estimation of cast iron materials. Procedia Eng 2010;2(1):1283–90.

[75] Gorash Y, MacKenzie D. On cyclic yield strength in definition of limits for characterisation of fatigue and creep behaviour. Open Engineering 2017;7(1): 126–40.

[76] Nieslony A, Bohm M. Mean stress effect correction using constant stress ratio S-N curves. Int J Fatigue 2013;52:49–56.

[77] Puigoriol-Forcada JM, Alsina A, Salazar-Martín AG, Gómez-Gras G, Pérez MA. Flexural fatigue properties of polycarbonate fused-deposition modelling specimens. Mater Des 2018;155:414–21.

[78] Zhang C, Chen H, Huang T-L. Fatigue damage assessment of wind turbine composite blades using corrected blade element momentum theory. Measurement 2018;129:102–11.

[79] Zheng T, Zhao C, He J. Research on fatigue performance of offshore wind turbine blade with basalt fiber bionic plate. Structures 2023;47:466–81.

[80] Susmel L, Tovo R, Lazzarin P. The mean stress effect on the high-cycle fatigue strength from a multiaxial fatigue point of view. Int J Fatigue 2005;27(8):928–43.

[81] Mecséri BJ, Kövesdi B. Discussion on the Hot-Spot and Notch Stress Based Fatigue Assessment Methods Based on Test Results. International Journal of Steel Structures 2020;20(4):1100–14.

[82] Lee J-M, Seo J-K, Kim M-H, Shin S-B, Han M-S, Park J-S, et al. and M. Int J Nav Archit Ocean Eng 2010;2(4):200–10.

[83] Haghpanahi M, Pirali H. Hot Spot Stress Determination for a Tubular T-Joint under Combined Axial and Bending Loading. International Journal of Industrial Engineering & Production Research 2006;17:21–8.

[84] Hobbacher A. The new IIW recommendations for fatigue assessment of welded joints and components – A comprehensive code recently updated. Int J Fatigue 2009;31(1):50–8.

[85] Huang Z-Y, Zhang W, Qian X, Su Z, Pham DC, Sridhar N. Fatigue behaviour and life prediction of filament wound CFRP pipes based on coupon tests. Mar Struct 2020;72:102756.

[86] IBM, *IBM SPSS Statistics for Windows*. 2021, IBM Corp: Armonk, NY.

[87] Freedman, D.A., *Statistical models: theory and practice*. 2009: cambridge university press.